Title

Modification of Model Boats for Open Water Testing of Drag Reducing Surfaces

Author

Carter, Christopher Mahlon

Publication Date

2022

Peer reviewed|Thesis/dissertation

UNIVERSITY OF CALIFORNIA

Los Angeles

Modification of Model Boats for Open Water Testing of Drag Reducing Surfaces

A thesis submitted in partial satisfaction

of the requirement for the degree Master of Science

in Mechanical Engineering

by

Christopher Mahlon Carter

2022

ABSTRACT OF THE THESIS

Modification of Model Boat for Open Water Testing of Drag Reducing Surfaces

by

Christopher Mahlon Carter

Master of Science in Mechanical Engineering

University of California, Los Angeles, 2022

Professor Chang-Jin Kim, Chair

Superhydrophobic (SHPo) surfaces coated on the hulls of marine vessels are capable of passively producing drag reduction. This gives SHPo technology an exciting opportunity to dramatically reduce the fuel costs and pollutant emissions of large ships or increase the top speeds of racing boats. While the performance of SHPo surfaces in laminar flow is now well understood and predictable, their performance in turbulent conditions is still faced with lack of knowledges and many uncertainties. Furthermore, most experimental studies in turbulent flow have been conducted in laboratory conditions, which often produce over-optimistic results when compared to the open-

water environment in the field conditions. This thesis creates a convenient method to test SHPo surfaces covering the hull of a watercraft in realistic conditions, by comparing the speeds of two identical model boats, whose hulls are attached with smooth or SHPo surfaces, under fully turbulent flows in the open water of a lake. With the molded SHPo samples the UCLA Micro & Nano Manufacturing Laboratory is developing in mind, this thesis aims to confirm that the boat operator can reliably drive the developed model boats at the same speed for a given throttle. At 75% throttle, the two model boats both travel steadily at 1.9±0.2 m/s with $Re_x = (7.2\pm0.9)\times10^5$, yielding a speed difference of 0%. At 100% throttle, the two boats travel steadily at 10.3±0.2 m/s with $Re_x = (3.6\pm0.2)\times10^6$ and 10.5±0.2 m/s with $Re_x = (3.7\pm0.2)\times10^6$, yielding a speed difference of 2%. Additionally, this research takes the first steps of considering the real-world potential of SHPo drag reduction by estimating the cost and value of the molded SHPo surfaces as a commercial product. The return on investment (ROI) for implementing SHPo surfaces on a cargo ship hull is estimated to be between 338% and 562%, depending on the material used to fabricate the SHPo surfaces.

The thesis of Christopher Mahlon Carter is approved.

Jeffrey D Eldredge

Kunihiko Taira

Chang-Jin Kim, Committee Chair

University of California, Los Angeles

2022

Thank you, Professor CJ Kim, for your wisdom and guidance. Thank you, Francisco Jose del Campo Melchor and Alexander McClelland, for aiding me in my experiments. It has truly been a pleasure to work with everyone in the UCLA Micro & Nano Manufacturing Laboratory.

Table of Contents

List of Figures

List of Tables

Chapter 1: Introduction and Motivation

1.1 Motivation

Superhydrophobic (SHPo) surfaces have been studied intensively for the last 20 years due to their ability to produce hydrodynamic drag reduction and protect surfaces from biofouling, corrosion, and icing [1]-[7]. SHPo surfaces capable of producing hydrodynamic drag reduction in turbulent flows are especially important, since drag reduction on marine vessels could dramatically reduce the fuel costs and pollutant emissions of watercraft [8]-[10]. SHPo surfaces can maintain their drag reducing properties passively, meaning that once SHPo surfaces are coated on the hull of a marine vessel, they can increase the vessel's top speed and fuel-efficiency without requiring a continuous supply of energy or material to operate [8]. The performance of SHPo surfaces in laminar flow is well understood and predictable as of 2010, but their performance in turbulent conditions is not yet certain [8], [11]. This paper introduces a new method for SHPo surfaces to be tested in open-water, turbulent flows using small model boats. This paper also takes the first steps for assessing the future of SHPo surfaces as a commercial product, by estimating the return on investment (ROI) for coating SHPo surfaces on cargo ships and discussing the use of roll-to-roll (R2R) manufacturing to mass-manufacture SHPo surfaces.

1.2 Defining a Superhydrophobic Surface

A hydrophobic surface is a surface that repels water. By definition, a hydrophobic surface has a contact angle of water that is greater than 90 degrees. Conversely, a hydrophilic surface is a surface that is easily wetted by water and has a contact angle of water that is less than 90 degrees.

This contact angle is measured from within the liquid. It is produced by the energy balance at the triple point between the liquid-solid interface, liquid-gas interface, and solid-gas interface to create thermodynamic equilibrium [12]. This concept is illustrated in Figure 1.1.

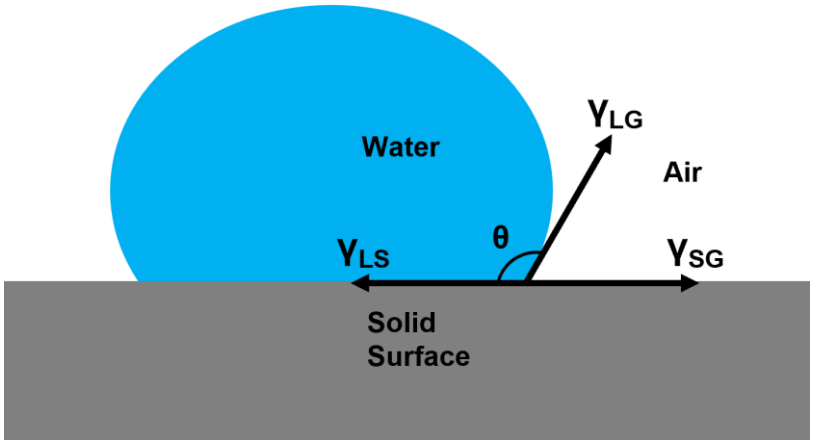

Figure 1.1: A water droplet in air on a hydrophobic solid surface has a contact angle θ larger than 90 degrees. The contact angle is a product of the thermodynamic equilibrium of the three interfaces. There exists a homogenous liquid-solid interface between the water droplet and the solid surface. Figure modified from the graduate course Microsciences (UCLA MAE 281), courtesy of Professor CJ Kim.

The contact angle θ of a water droplet on a smooth surface is given by the Young equation, shown in Equation 1.1, where γ_{SG}, γ_{LS}, and γ_{LG} are the surface tension of the solid-gas interface, liquid-solid interface, and liquid-gas interface, respectively.

$$\cos\theta = \frac{\gamma_{SG} - \gamma_{LS}}{\gamma_{LG}} \tag{1.1}$$

Taking hydrophobicity even further, a superhydrophobic (SHPo) surface is a surface with a contact angle of water that is greater than 150 degrees and a small (e.g., smaller than 10 degrees) contact angle hysteresis or tilt angle. SHPo surfaces are fabricated by combining the inherent hydrophobic properties of certain materials (e.g., Teflon) with surface roughness [8]. Hence, a SHPo surface is created either by roughening the surface of a hydrophobic material or by coating a thin hydrophobic material onto a rough surface [3], [13], [14]. Surface roughness can come in different forms, such as random roughness, microscopic trench structures, or microscopic post structures, as illustrated in Figure 1.2. In contrast to a smooth surface, which only possesses an intrinsic contact angle, a rough surface has both an intrinsic contact angle θ and an apparent contact angle θ^* [15]. The intrinsic contact angle is the contact angle measured along the physical surface of the surface's likely non-planar roughness, at the microscopic view. The apparent contact angle is the contact angle measured at the macroscopic view along the seemingly flat surface of the rough surface.

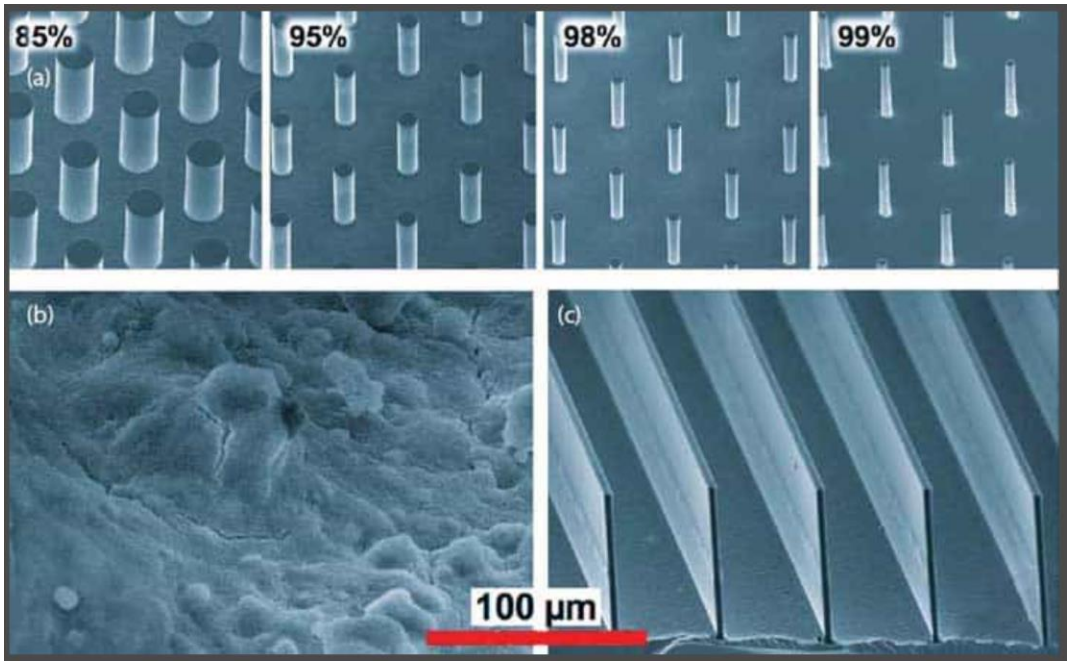

Figure 1.2: (a) The microscopic post structures of a SHPo surface, made with various gas fractions (i.e., the top layer of the surface is 85% gas and 15% solid). (b) A SHPo surface with random roughness. (c) A SHPo surface made of microscopic trenches. Scale bar applies to all sections. Figure duplicated from [13].

If a surface is fully wetted by water, meaning that no gas exists in between the homogenous liquid-solid interface, then that surface is said to be in the Wenzel state [12]. If the surface is either partially wetted or not wetted, meaning that there is either a heterogeneous liquid-gas and liquid-solid interface, or that there is a layer of gas in between the free surfaces of the liquid and solid, then the surface is said to be in the Cassie-Baxter state [16]. The Cassie-Baxter state is illustrated in Figure 1.3.

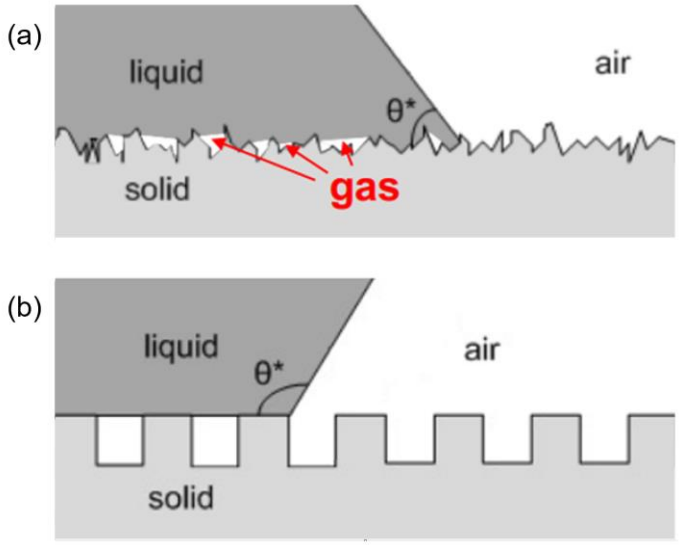

Figure 1.3: (a) A surface with random roughness in the Cassie-Baxter state with a heterogeneous liquid-gas and liquid-solid interface. (b) A surface with regular roughness (e.g., microscopic trenches or posts) in the Cassie-Baxter state with a heterogeneous liquid-gas and liquid-solid interface. Figure duplicated from the graduate course Microsciences (UCLA MAE 281), courtesy of Professor CJ Kim.

1.3 Drag Reduction with SHPo Surfaces

When immersed in water, a SHPo surface may passively trap a thin layer of gas, called a plastron, on its outer surface [8]. If the plastron is maintained, the SHPo surface exists in the Cassie-Baxter state while submerged. This plastron acts as a lubricating barrier between the solid SHPo surface and the water flowing across it [13]. While a liquid-solid interface possesses a no-slip condition, the liquid-gas interface of the plastron possesses an effective slip that reduces skin friction drag [8]. The drag reduction caused by the SHPo surface is determined by the amount of

effective slip, which is dependent on the pitch of the microstructures of the surface roughness, the gas fraction of the heterogenous interface of the plastron, and the pattern type (e.g., trenches, posts, random roughness) [11]. The effective slip is described by a slip length δ that is obtained by extrapolating the slip velocity u_s below the SHPo surface, as is shown in Figure 1.4 [8]. In Navier's model of the slip boundary condition, the magnitude of the slip velocity u_s is proportional to both the magnitude of the shear rate $\partial u/\partial y$ experienced by the fluid at the wall ($y = 0$) and to the slip length δ, as is shown in Equation 1.2 [8], [17].

$$u_s = \delta \left| \frac{\partial u}{\partial y} \right|_{y=0} \tag{1.2}$$

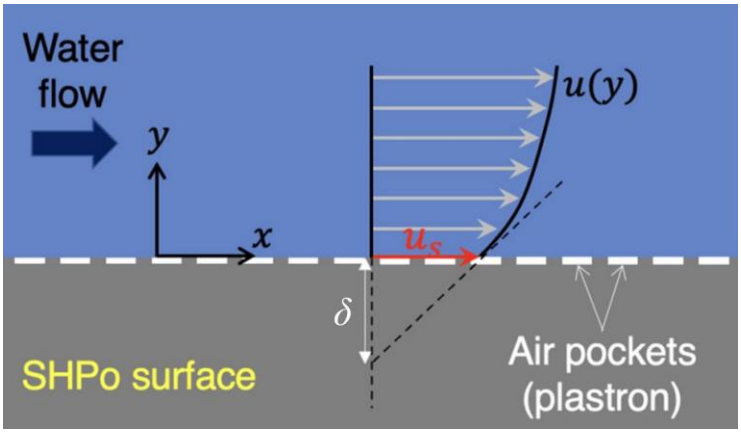

Figure 1.4: Velocity distribution on a SHPo surface, showing a slip velocity u_s and an effective slip length δ. Figure adapted from [8].

Smooth hydrophobic surfaces with no plastron are also capable of producing an effective slip, but the size of the slip length is too small to cause significant drag reduction in regular-sized flows [11]. Ideally, a flat hydrophobic surface would hold a uniform gas layer across its surface, as shown in Figure 1.5. For this uniform gas layer, the slip length can also be calculated using Equation 1.3, where H is the thickness of the gas layer, η_{liquid} and η_{gas} are the liquid and gas viscosities [11]. It is assumed that there is continuity of shear stress at the liquid–gas interface.

$$\delta = H\left(\frac{\eta_{liquid}}{\eta_{gas}} - 1\right) \tag{1.3}$$

However, in reality, the uniform plastron on a flat surface would be sheared away by the water flow [11]. Instead, the plastron can be stably maintained within the microstructures of a SHPo surface. Whereas a uniform gas plastron has a homogenous liquid-gas interface with a slip condition present throughout the interface, the plastron maintained within the SHPo microstructures has a heterogenous liquid-gas and liquid-solid interface with certain locations possessing the no-slip condition, due to the top surfaces of the microstructures being exposed to the liquid (see Figure 1.5). This causes the slip length of the plastron in the micro-structured surface to be smaller than that of the theoretical uniform gas layer. Despite this fact, the drag reduction caused by the plastron in micro-structured surfaces was found to be large enough when compared to smooth surfaces to be of practical significance [1], [2], [11], [18]-[20].

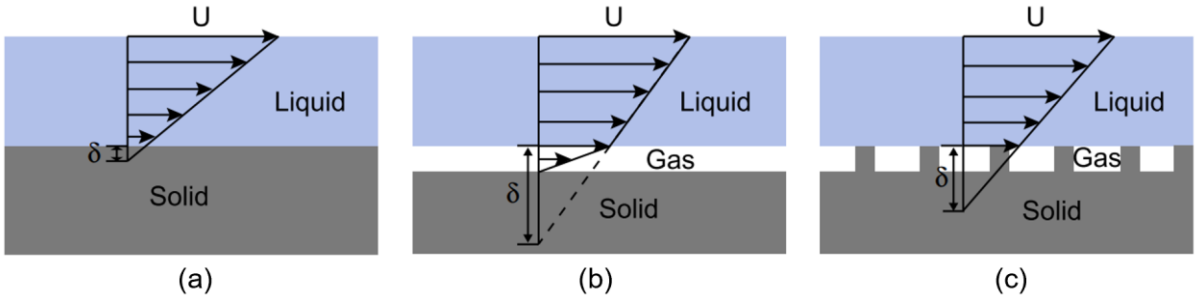

Figure 1.5: Effective slip modeled on (a) a flat hydrophobic surface with no plastron and negligible slip length, (b) a flat hydrophobic surface with a theoretical uniform plastron, and (c) a micro-structured SHPo surface with plastron existing within its surface roughness. Figure duplicated from [11].

For laminar flow experiments, drag reduction (*DR*) by a liquid slip in Couette flow can be calculated using Equation 1.4, where *H* is the gap distance between the slip surface (liquid-gas interface) and the opposing non-slip surface (liquid-solid interface) [11], [20].

$$DR = \frac{1}{\left(1+\frac{H}{\delta}\right)} \tag{1.4}$$

The drag reduction of liquid slip in Poiseuille flow is shown in Equation 1.5 [1], [11], [20].

$$DR = \frac{3}{\left(3+\frac{H}{\delta}\right)} \tag{1.5}$$

Note that a SHPo surface must have a large slip length to produce large drag reduction, meaning it must sustain its gas plastron. Having a hydrophobic contact angle is simply a necessary condition

to be capable of drag reduction. When a single water droplet rests atop a SHPo surface in the Cassie-Baxter state, the air residing within the microstructures or random roughness is exposed to the surrounding atmosphere, which provides an infinite supply of air and keeps the air under the droplet at atmospheric pressure. However, in the case of a SHPo surface being submerged underwater, the air supply within the microstructures is finite and the air plastron is compressed by the water. Consequently, the Cassie-Baxter state is fragile underwater. If the hydrostatic pressure is too large, the meniscus of the liquid-gas interface is deformed, and the plastron is squeezed into the microstructure. If the meniscus of the plastron within the microstructure is deformed enough to exceed the advancing contact angle of the sidewall, then water will penetrate the plastron and wet the SHPo surface [11], [21]. If the gas concentration of the surrounding water is too low, such that the partial pressure of the air saturated in the water is less than the air pressure of plastron, then air will diffuse from the plastron into the water, depleting the plastron over time [21]. As the plastron is deformed or depleted, the effective slip and drag reduction effect is reduced [11]. Additionally, since the water flow across the SHPo surface is not static in practical applications, the shear stress applied on the liquid-gas interface by the flowing water will drag the air in the plastron along with it [7]. This increases the air pressure at the downstream end of the microstructure, creating a pressure flux within the plastron, as shown in Figure 1.6. If either the upstream or downstream ends of the deformed plastron exceeds the advancing or receding contact angle of the sidewall, respectively, then the plastron is lost [7].

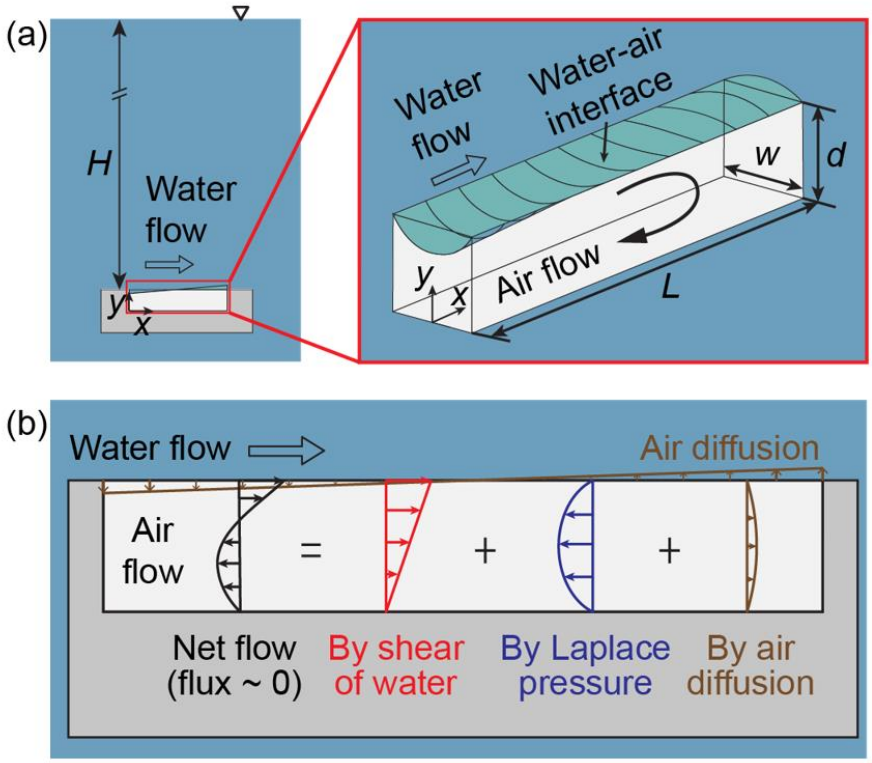

Figure 1.6: Pressure flux created within the plastron as a result of the shear force of the external water flow. This phenomenon is known as the shear drainage effect. (a) Illustration of the deformation of the plastron and the air flow inside the plastron. (b) 2D profiles of the *x*-direction air flow inside plastron. Figure duplicated from [7].

1.4 Testing SHPo Surfaces in Laminar and Turbulent Flows

Initially, experimental studies of both regular structures (e.g., trenches, posts) and random roughness in laminar flows found inconsistent slip length results [1], [2], [11], [18], [20], [22]-[51]. Some early literature studying structurally similar SHPo surfaces measured slip lengths that differed significantly from the results of other papers [11], [24], [28]. Ultimately, it was found that

the inconsistent results of these early papers were due to the fact that the depletion of the plastron on their tested SHPo surfaces was not closely monitored [8], [11].

Since randomly structured surfaces are simpler to manufacture than regularly structured surfaces, they have been a popular choice in many experimental studies [11]. Unfortunately, a trend of deteriorating drag reduction over time is consistently reported throughout all experiments using randomly structured surfaces [11]. This is a result of random roughness surfaces' inability to maintain their plastron long-term [8], [11], [21], [52]. Initially, the pitch between the locations at which the water pins to the top surface of the roughness microstructures is very large, yielding strong drag reduction. However, the pitch decreases over time as the plastron diminishes, as illustrated in Figure 1.7. Decreasing pitch leads to decreasing slip length and drag reduction, until both the plastron and any drag reduction are lost completely [11]. Successful drag reduction with random roughness has not been shown in any turbulent flow tests, ultimately showing that random roughness will very likely not work for real-world practical applications [8].

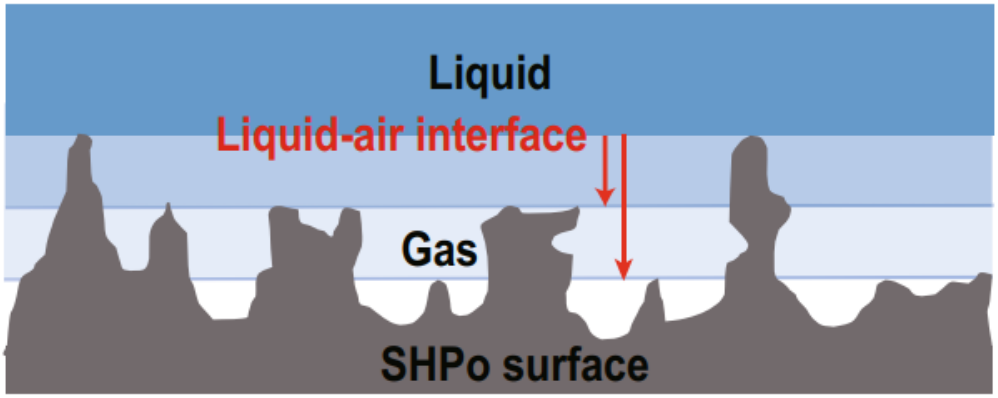

Figure 1.7: Gradually depleting plastron on a random roughness SHPo surface causes pitch, and consequently drag reduction, to decrease over time. Figure duplicated from [11].

Many experimental studies have also been conducted on regularly structured SHPo surfaces (e.g., trenches, posts) [11]. Regularly structured SHPo surfaces are often manufactured using a photolithography process, such as the process flow shown in Figure 1.8 [52]. The consensus of the studies performed thus far is that for both laminar and turbulent flows, micro-trenches that face longitudinally to the oncoming water flow are the most effective surface structure for producing slip length and drag reduction, when compared to transverse trenches, post structures, and random roughness [8], [11], [21]. In fact, longitudinal microtrenched SHPo surfaces of large slip lengths have been reported to cause drag reductions as much as 75% in turbulent boundary layer flows, tested in a water tunnel [53].

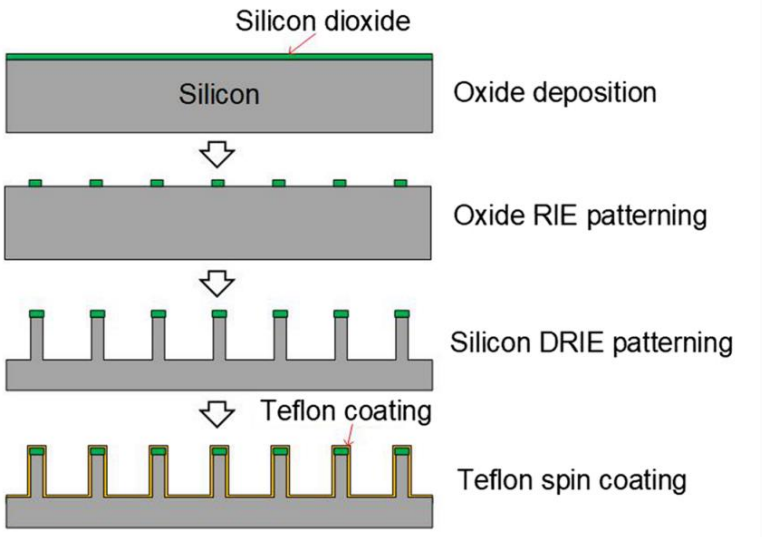

Figure 1.8: Micro-fabrication process flow using deep reactive ion etching (DRIE) to create the micro-trenches of a regularly structured SHPo surface. Figure duplicated from [52].

For laminar flow studies, the slip length can be obtained directly from the velocity profile, which is optically probed on a SHPo surface, or through indirect methods such as measuring the flow rate or shear stress [11]. While the effective slip and drag reduction of SHPo surfaces in laminar flows are relatively well understood now, the effective slip in turbulent flows is still uncertain [11]. In turbulent flow, there is a wide range of scales that affect the skin friction drag (such as the lack of a self-similar boundary layer, and the need to use analytically derived equations that are difficult to acquire) which make it difficult to establish a universal relation between the drag reduction and slip length of a SHPo surface [8]. Numerical studies of turbulent flows have shown definite drag reduction, but experimental studies have shown results ranging from significant drag reduction to negligible drag reduction, and even drag increase [8], [52], [54]-[57]. Currently, it is predicted that the cause of misleading turbulent flow studies is a depleted plastron, similar to the case with early laminar flow studies [8]. In fact, the plastron is even more fragile in turbulent flows than laminar flows, due to the increased shear stress, inertia, and pressure fluctuation of turbulent flows, especially at high Reynolds numbers [8], [58]-[60].

When it comes to measuring drag reduction in turbulent flow, the equations (e.g., Equation 1.4, Equation 1.5) and measurement methods for laminar flow do not hold. Instead, shear stress is measured so that drag reduction can be acquired using empirical equations [52].

Turbulent flow studies on SHPo drag reduction have predominantly used water tunnels as their measurement devices [13], [52]. However, the confined flow of water tunnels can lead to over-optimistic results, since the confined flow can quickly become supersaturated with air, causing a larger and more stable plastron than what would be experienced in open-water flow, which typically has undersaturated water [8], [13]. Consequently, some of the few studies that tested in the open-water flows of tow tanks reported a drag increase when using random roughness [13], [61]. Other experiments that were performed in open-water conditions tested SHPo surfaces by coating them on model boats [62]-[64]. However, the characteristic length of the model boats used in these studies were in the magnitude of centimeters, and they only traveled at low speed (< 0.5 m/s), so they did not reach a high enough Reynolds number to achieve the turbulent flows of practical interest [52], [62]-[64]. Thankfully, new studies for turbulent flows performed at UCLA have developed a way to measure the drag reduction of SHPo samples in high-speed, open-water conditions by differentially measuring shear stress of a SHPo sample compared to that of a baseline non-SHPo smooth sample. These studies measure drag reduction by mounting a custom shear sensor underneath the hull of a 13-foot-long motorboat, which is driven at speeds of up to 6 m/s [52]. It is important to test SHPo surfaces in real marine environments, rather than only laboratory conditions, because real-world water contains pollutant chemicals, surfactants, and biofouling, which all adversely affect the health of the plastron. Encouragingly, these open-water studies have shown drag reduction of up to 30%, showing promise for the future of SHPo surfaces in real-world, practical applications [8], [52].

1.5 Financial Assessment of SHPo Surfaces

On top of testing and improving newly developed SHPo samples, it is also important to study the economy of implementing SHPo surfaces as a commercial product in the future. When it comes to developing methods of mass-manufacturing SHPo surfaces, most of the procedures proposed thus far have been concerned only with producing random roughness structures [8], [65]-[67]. However, some methods of mass-producing regularly structured SHPo surfaces have also been proposed, predominantly using hot embossing and roll-to-roll manufacturing [8], [68]-[72]. In this paper, the financial future of SHPo surfaces is investigated by making estimates for the cost of goods (COG) and return on investment (ROI) of SHPo surfaces on a typical cargo ship, using the limited information we have thus far regarding a business plan.

1.6 Development of Model Boats to test SHPo Surfaces

Unfortunately, the procedure for testing the drag reduction of SHPo samples on the 13-foot motorboat is both time-consuming and expensive. Additionally, only a single 4 cm by 7 cm SHPo sample is tested at a time, meaning that the sample only makes up a small percentage of the motorboat's hull area. Hence, the SHPo surface does not ultimately impact the performance of the boat itself. It is a concern that once an entire vessel is coated with these slippery SHPo surfaces covered with plastron, the overall hydrodynamics and maneuverability of the vessel may be affected in ways that have not yet been considered [8]. In this paper, a new experimental process is introduced that uses small model boats to test SHPo samples in high-speed, open-water conditions. This way, newly developed SHPo samples can be tested conveniently and affordably.

If the SHPo samples show promise of beneficial drag reduction on the small model boats, the samples can then be taken to the motorboat shear-sensor test to acquire accurate drag reduction data. This model boat approach also allows the SHPo surfaces to showcase their drag-reducing benefits by affecting the top speed performance of the boats. While other experiments using small model boats were only able to test in speeds of up to 0.5 m/s, the model boats used in this study are capable of reaching top speeds of roughly 10 m/s [62]-[64]. Additionally, while other model boat experiments used boats or submarines that were at most about 1 foot long, the boats used in this study have a characteristic length of roughly 18 inches [62]-[64]. The samples are tested in turbulent flow with a Reynolds number of roughly $Re_x = 3.6 \times 10^6$, which is a Reynolds number that is high enough to be applicable to real-world engineering purposes.

Chapter 2: The Benefits and Costs of Implementing Superhydrophobic Drag Reduction

2.1 Market Analysis

2.1.1 Motivation

To assess the profitability of micro-trenched SHPo surfaces as a commercial product, it is necessary to calculate an estimated return on investment (ROI) for the application of SHPo surfaces. For initial cost estimates during the early development of a business strategy, the unit costs of the product are more critical to consider than the fixed costs. The dominating unit costs in calculating the cost of goods (COG) of SHPo surfaces are material costs, manufacturing costs, and installation costs.

2.1.2 Benefit of Drag Reduction in Cargo Shipping

SHPo technology can provide substantial value in nearly any industry involving watercraft, due to its ability to passively reduce frictional hydrodynamic drag [8]. The shipping container industry is one of the largest industries in the world, bringing in billions of dollars of revenue every year, yet also spending significant amounts of money on fuel-oil. AP Moller-Maersk, one of the largest shipping companies in the world, brings in roughly $30 billion of revenue annually but spends nearly $4 billion on fuel-oil [73], [74]. Hence, roughly 13% of annual revenue is lost on fuel-oil costs. Additionally, the shipping industry as a whole accounts for 3.1% of the annual global CO_2 emissions, 7% of annual global NO_x emissions, and 4% of annual global SO_x emissions [9], [75]. This provides drag reducing SHPo surfaces an exciting opportunity to significantly lower the operating costs and pollutant emissions of cargo ships.

2.1.3 Fuel Savings by SHPo Drag Reduction on Cargo Ships

On average, a containership consumes 26,000 metric tons of fuel-oil annually [9]. During operation, frictional drag of water flows accounts for 60%–70% of the total drag on the hull of a cargo ship [75]. The SHPo surfaces manufactured by the UCLA Micro & Nano Manufacturing Laboratory have achieved drag reduction of 30% in an actual marine environment at the high Reynolds numbers of practical interest [52]. Expecting the overall drag reduction to be lower in practice, a conservative estimate of 15% reduction of friction drag will be used. Hence, the application of SHPo surfaces onto a cargo ship hull can reduce total drag on a cargo ship by around 10%, which would reduce the amount of fuel-oil used by a cargo ship by about 2,500 metric tons annually. The price of marine fuel-oil fluctuates over time, and it is difficult to predict its future price. The fuel-oil most commonly used by containerships since 2020, called VLSFO, has cost $600 per metric ton on average since January 2020 [76]-[80]. Hence, the reduction of fuel-oil consumption by a typical cargo ship due to drag reducing SHPo surfaces can save roughly $1.4 million annually.

2.1.4 Estimating the Wetted Surface Area of a Typical Cargo Ship

To estimate the cost of applying SHPo on a cargo ship, it is first necessary to estimate the amount of SHPo surfaces need to coat its hull. The most common class of container ship by number is the Handysize bulk carrier, a medium sized container ship with a carrying capacity of up to 40,000 deadweight tonnage (DWT) [81], [82]. In 2015, Handysize vessels made up 71% of all bulk carriers above 10,000 DWT, owing their popularity to their ability to access a wide range of ports all around the world [83]. While specific Handysize-class vessels have varying dimensions, an upper-limit estimate of a Handysize's length, beam, and draft are 150 meters, 20 meters, and

10 meters, respectively [83]-[85]. Due to the complex geometry of container ship hulls and the fact that different vessels within the same class have varying dimensions, calculating the wetted surface area of the average container ship relies on estimations. For a very rough estimate of the wetted surface area of a container ship, Equation 2.1 can be used

$$A = L(B + d) \tag{2.1}$$

where A is wetted surface area, L is the overall length of the vessel, B is the vessel's beam, and d is the vessel's draft [86], [87]. For an estimation of wetted surface area that better accounts for the hull curvature, bow bulb, and other geometric parameters of cargo ship hulls, Equation 2.2 can be used

$$A = L(B + 2d)C_M{}^{0.5}(0.4530 + 0.4425C_B - 0.2862C_M - 0.003467\frac{B}{d} + 0.3696C_{WP}) + 2.38\frac{A_{BT}}{C_B} \tag{2.2}$$

where C_M is midship coefficient, C_B is blocking coefficient, C_{WP} is waterplane coefficient, and A_{BT} is bulb area percentage [88]. Estimates for the coefficients and bulb area percentages for different vessel types are acquired from the data published by The Society of Naval Architects and Marine Engineers [88], [89]. Utilizing Equation 2.1 and Equation 2.2 to calculate the wetted surface area of a Handysize containership results in estimates of 4500m^2 or 3880m^2, respectively. The larger estimate of 4500m^2 is used for this cost analysis to ensure a conservative estimate for the ROI of SHPo surfaces.

2.1.5 Material Costs of trench SHPo Films

Although the trench SHPo samples developed for the experiments so far have been made on silicon wafers for scientific studies, silicon SHPo surfaces would be prohibitively expensive for adoption in practice [52, 53, 90]. When SHPo surfaces are applied to watercraft commercially, they will likely need to be fabricated by a mass manufacturing method using a flexible material. While the best choice for such a material is still being investigated, the most desirable materials are low-cost, flexible, durable, and inherently hydrophobic. The promising options under consideration include Teflon (PTFE), fluoroacrylate polymer, and polydimethylsiloxane (PDMS), with Formlabs Flexible 80A Resin as a specific material used in the UCLA Micro & Nano Manufacturing Laboratory. After reaching out to many suppliers for the bulk-order prices of these chemicals, the estimate costs have been acquired and are reported in Table 2.1. The communications with suppliers regarding pricing are collected in the Appendix section.

Table 2.1: Bulk Order prices of possible choices for flexible SHPo substrate materials. More information regarding bulk-order costs is available in the Appendix.

Chemical Name	Price ($/gallon)
PDMS	69.18
PTFE	80.89
80A Resin	527.31
Fluoroacrylate	532.71

It is assumed that the type of SHPo surfaces applied to cargo ship hulls will be micro-trenched SHPo surfaces, since this type of structure has been shown to be the most effective at producing beneficial drag reduction thus far [8], [11], [21], [53]. While the exact dimensions of these micro-trenches vary from study to study, the dimensions of the micro-trenched SHPo surfaces currently fabricated at the UCLA Micro & Nano Manufacturing Laboratory follow the dimensions shown in Figure 2.1. Increasing the pitch and gas fraction of the trenches produces a larger slip length, but results in a plastron that is more easily lost. A pitch of 100 μm and gas fraction of 90% have been found to offer a good balance between drag reduction and plastron stability. The substrate thickness of 300 μm is chosen because a larger thickness increases manufacturing costs, but a substrate that is too thin will tear during the demolding step. Samples are currently fabricated to be 4 cm by 7 cm to fit the shear sensor of the laboratory's current drag reduction testing method [52]. When mass-produced, the same SHPo trench structure can be extrapolated beyond a 4 cm by 7 cm area. In reality, the edges of the trenches will be closed off to retain the plastron, but for now it is assumed that a unit area of the larger SHPo surface will follow the structure shown in Figure 2.1. Hence, a 1 m^2 unit area of the vessel's hull would be covered with the micro-trench SHPo surface made from 3.09×10^{-4} m^3 (or 0.0816 gallons) worth of volume of a raw material.

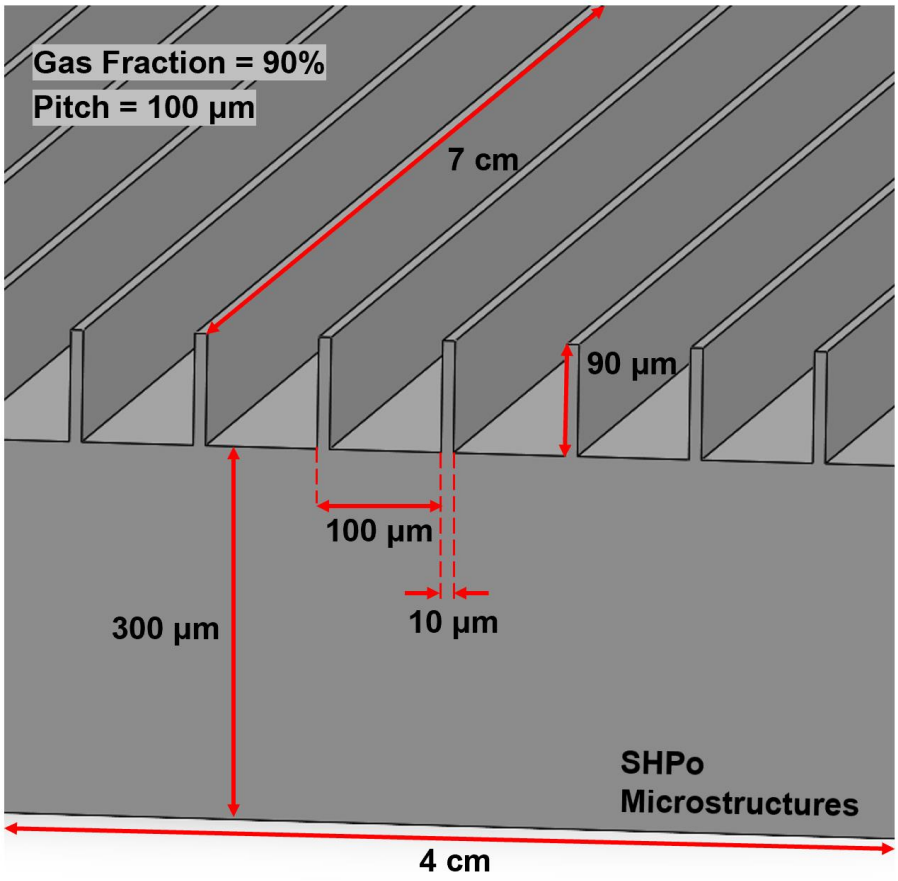

Figure 2.1: Diagram of SHPo micro-trench structures that illustrates the dimensions of the trenches, which have a trench pitch of 100 µm, trench depth of 90 µm, and a trench width of 90 µm. The bottom layer of the substrate is 300 µm thick.

2.1.6 Cost of Roll-to-Roll Manufacturing to Produce Trench SHPo Films

The large cargo vessels used in the shipping industry require a dauntingly large area of their hulls to be covered with SHPo surfaces. While it is evident that the commercial applications of SHPo technology involve hull surfaces in the magnitude of tens to thousands of square meters, the size of the SHPo samples manufactured for current experiments are merely in the magnitude

of square centimeters. A promising method that may be used to bring SHPo surfaces to high-volume production is the roll-to-roll (R2R) manufacturing method [66], [68], [69]. The process of R2R manufacturing works by continuously coating and patterning a material onto a flexible substrate film, where the substrate film is fed through a roller-based processing line [91]. Some of the rollers in the processing line are wrapped with the substrate film and drive the film through the assembly process. Either slot dies or additional rollers act as patterned molds that are filled with resin, which apply the resin onto the substrate film as the film passes through the processing line [92]. Utilizing the R2R manufacturing method, SHPo surfaces can be mass manufactured on a wrapped film, which can then be applied to a ship's hull. A diagram illustrating an anticipated method of using R2R manufacturing to create films of micro-trenched SHPo surfaces is shown in Figure 2.2. SHPo microstructures will be cured atop a backing film, with an acrylate pressure sensitive adhesive and a release liner applied to the other side of the backing film. It is estimated that the backing film/liner and adhesive will cost roughly \$32.27/m^2 and \$111.18/gal, respectively [93], [94]. On a relatively smooth surface, one gallon of adhesive can cover roughly 30 m^2 [95].

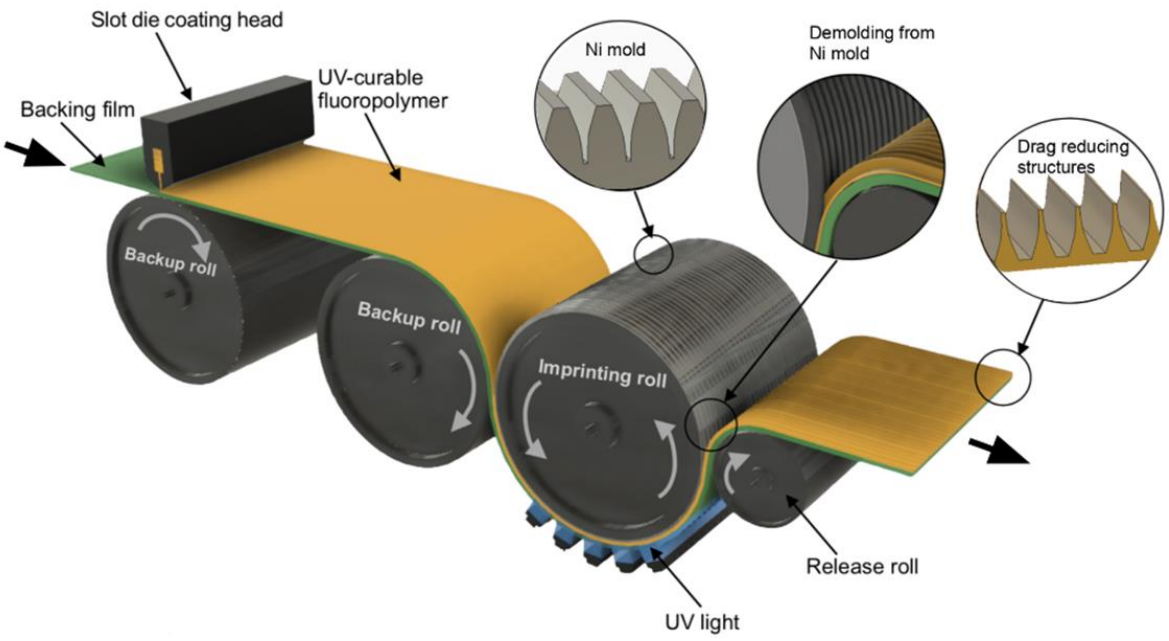

Figure 2.2: Anticipated MEMS-based roll-to-roll manufacturing method to create micro-trenched SHPo surfaces. Figure courtesy of Tracy Liu of the UCLA Micro & Nano Manufacturing Laboratory.

The R2R manufacturing method has already been successfully used to rapidly manufacture riblet film, which shows promise for mass-manufacturing of SHPo surfaces by R2R manufacturing. Riblet film is similar to micro-trenched SHPo surfaces in that it uses micro-structured grooves that are patterned onto a substrate film to create passive drag reduction [96]. The German research institute Fraunhofer IFAM has designed and prototyped a R2R manufacturing device which applies a UV-curing lacquer to a substrate and cures the lacquer in the shape of a riblet microstructure, all in one single process [97]-[99]. The Fraunhofer IFAM riblet device is shown in Figure 2.3.

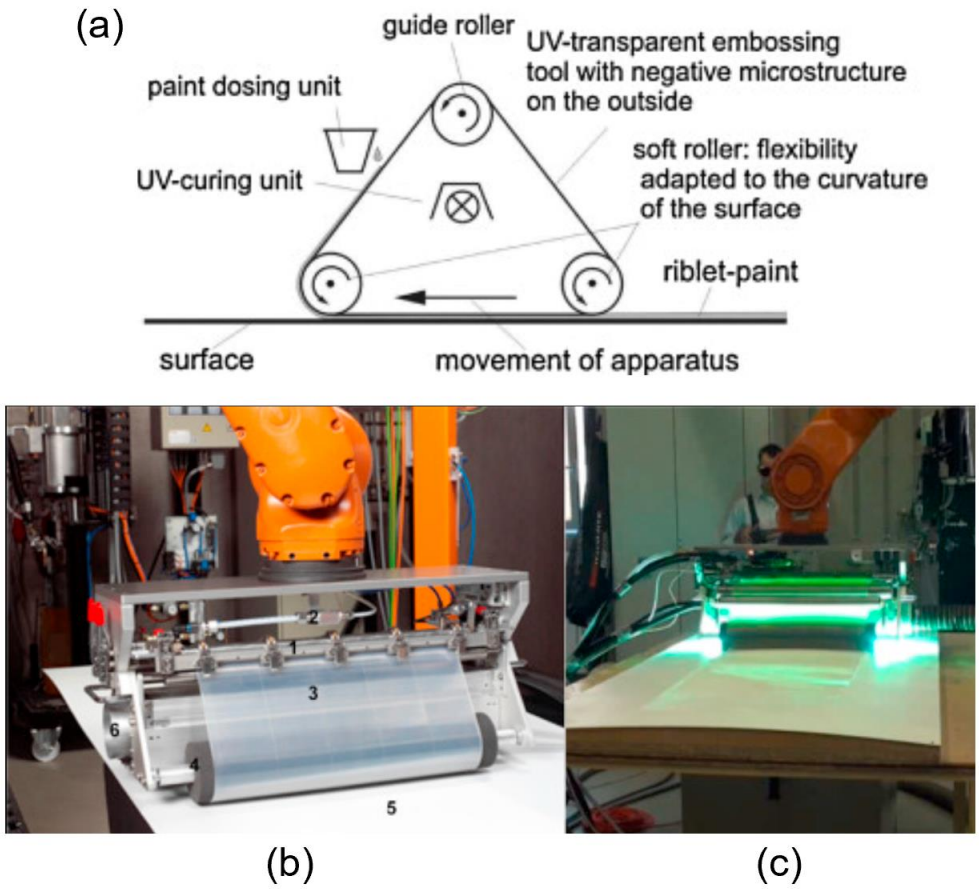

Figure 2.3: (a) Side-view diagram of Fraunhofer IFAM riblet embossing and curing device showing how various components of the device function. (b) The Fraunhofer IFAM riblet device mounted to a robot arm. (c) The Fraunhofer IFAM riblet device applies riblets to a surface with its mercury vapor lamp turned on. Figure 2.3a duplicated from [97]. Figure 2.3b and Figure 2.3c duplicated from [98].

The device is operated by using a slot nozzle to pour the UV-curing lacquer onto a transparent silicone film that is rolled about the guide rollers. The silicone film is the mold, possessing the negative microstructure of the riblets. After being wetted with lacquer, the silicone

film is rolled over the substrate surface, as the foam guide rollers press the lacquer against the substrate. With the lacquer compressed against the substrate and shaped into the three-dimensional riblet structure by the silicon mold, a mercury vapor lamp cures the lacquer from above, hardening and adhering the riblets onto the substrate. The motion of the device is continuous and can apply riblets at a speed of 1.5 m/min [99]. SEM images of the produced riblets are shown in Figure 2.4.

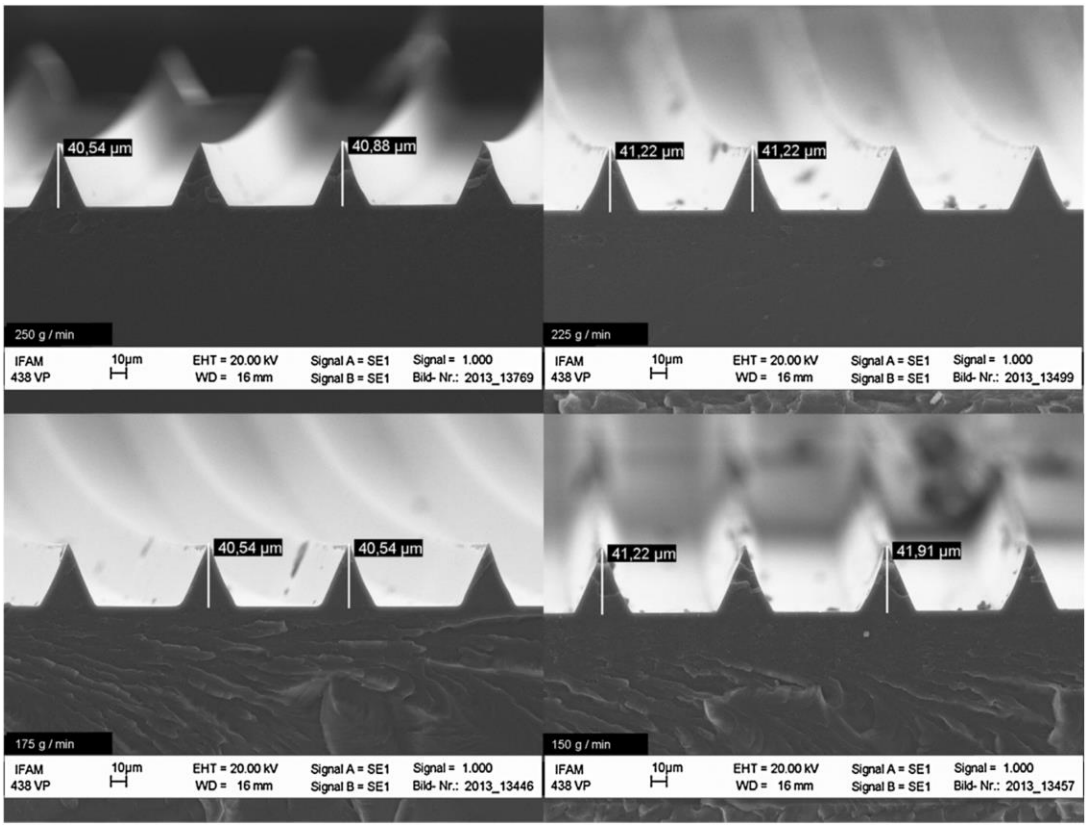

Figure 2.4: Riblets fabricated by the Fraunhofer IFAM roll-to-roll manufacturing device. Figure duplicated from [98].

To make estimates for the manufacturing costs of SHPo surfaces, it is assumed that the micro-trenched SHPo surfaces made for cargo ships in the future will be mass-manufactured using

a R2R machine or process line similar to those in Figure 2.2 or Figure 2.3. The power consumption of a R2R manufacturing machine is estimated to be 86 kW [100]. Since the cost of electricity in the state of California is roughly $0.20/kWh [101], the R2R manufacturing machine would cost $17.20/hour to run. Based on the speed of the Fraunhofer R2R machine (see Figure 2.3), it is estimated that the R2R process will print one-meter-wide rolls at a rate of 1.5 m/min, for a surface area production rate of 1.5 m^2/min [99]. Hence, for the 4500 m^2 estimated wetted surface area of the Handysize vessel, the R2R machine would need to run for 50 hours to manufacture SHPo surfaces for the full 4500 m^2 of hull area. It is assumed that 5 employees will operate the manufacturing facility and will be paid a wage of $60 per hour.

2.1.7 Installation Costs of SHPo Films on Cargo Ships

Installing SHPo surfaces onto the vessel's hull requires the work of boat painters or film applicators. Although it is difficult to determine exactly how many man-hours are required to complete the task, it is estimated that applying the SHPo surface onto a cargo ship will take roughly 2000 man-hours, based on the timeline of similar cargo ship hull painting and hull-repair projects [102]-[104]. The hourly wage of a SHPo product installer would likely be similar to the wage of a boat painter or vehicle wrap installer, who are paid an average hourly wage of $18.64 per hour or $26 per hour, respectively [105], [106]. A safe estimate of $30 per hour is used to calculate the wrap installers' wages for applying SHPo surfaces to the containership hull. To apply the SHPo film to the boat's hull, the ship must be taken into dry dock, in which the vessel is taken out of the water so parts of the ship that are typically underwater can be accessed. The cost of drydocking varies on the dock's location and the vessel's length. Based on the drydocking costs of ports in the

United States and United Kingdom with cargo ship repair capabilities, it is estimated that the cost of drydocking a typical Handymax vessel is at most $10,000 per day [107]-[109]. Note that this cost estimate is merely for parking the vessel in dry dock and does not include the cost of boat repair. Assuming the amount of time to apply SHPo surfaces to the cargo ship is similar to the timeline of a hull repair project, it is estimated that the vessel will need to stay in dry dock for seven days [103].

2.1.8 Administrative Costs of SHPo Films on a Cargo Ship

When a company sells SHPo films as a product, the company will need to make a profit margin to generate discretionary income and to cover administrative, transportation, and sales representative costs [110]. According to a report from New York University on the profit margins of U.S. companies, the average gross profit margin of companies in the shipbuilding and marine industry is 30.68% [111]. The gross profit margin can be used to calculate the total revenue that must be generated by a company from their sales, using Equation 2.3.

$$\text{Net Revenue} = \frac{\text{Cost of Goods}}{1 - \text{Gross Profit Margin}} \tag{2.3}$$

The net revenue earned from the sale of the product equals the product cost that is charged to the consumer, minus taxes, which is assumed to be 10% for boat purchases in the United States [112].

2.1.9 ROI of SHPo Drag Reduction on a Cargo Ship

The SHPo films on a cargo ship must be removed and replaced when the ship is brought into drydock for mandatory hull inspection and maintenance. Drydock hull inspections occur twice every five years, as is mandated by the United States Code of Federal Regulations regarding cargo vessels [113]. Extrapolating the estimated fuel-oil cost savings of a cargo ship ($1.4 million annually), SHPo surfaces save roughly $3.5 million in fuel-oil costs every 2.5 years. Using all of the assumptions and estimations that have been established thus far, the ROI of applying SHPo surfaces onto a Handysize vessel with a wetted surface area of 4500 m^2 is estimated for the cost of different substrate materials and summarized in Table 2.2. The ROI of applying SHPo surfaces to a typical cargo ship is estimated to be roughly 338% to 562%, depending on the substrate material used.

Table 2.2: Cost estimates for a typical container ship, assuming the trench SHPo surfaces are applied to a wetted surface area of 4500 m^2 and fabricated using either fluoroacrylate, PDMS, PTFE, or 80A Resin. (a) Cost of Goods, (b) Product Cost, and (c) Return on Investment.

	Unit Price	Quantity	Total Cost
Installation Costs			
Installer Wages	$30.00 /hour	2000 manhours	$60,000
Dry Docking	$10,000 /day	7 days	$70,000
Material Costs			
Substrate Material Options			
1. PDMS	$69.18 /gal	367 gal	$25,403
2. Teflon (PTFE)	$75.92 /gal	367 gal	$27,878
3. 80A Resin	$527.31 /gal	367 gal	$193,628
4. Fluoroacrylate	$532.71 /gal	367 gal	$195,611
Backing film & liner	$32.27 /m²	4500 m²	$145,215
Acrylic adhesive	$111.18 /gal	150.0 gal	$16,677
Manufacturing Costs			
Manufacturer Wages	$60.00 /hour	250 manhours	$15,000
Machine Operating Costs	$17.20 /hour	50.0 hours	$860
Cost of Goods Sold			
COG of Each Material Choice			
1. PDMS			**$333,155**
2. Teflon (PTFE)			**$335,630**
3. 80A Resin			**$501,380**
4. Fluoroacrylate			**$503,363**

(a)

	Total Amount
Total Commercial Product Cost	
Gross Profit Margin	30.68%
Sales Tax	10.00%
Investment Cost (Price for Consumer) of Each Material Choice	
1. PDMS	**$528,665**
2. Teflon (PTFE)	**$532,592**
3. 80A Resin	**$795,612**
4. Fluoroacrylate	**$798,759**

(b)

	Total Amount
Return on Investment	
Revenue (Lifetime Fuel Savings)	$3,500,000
ROI of Each Material Choice	
1. PDMS	**562%**
2. Teflon (PTFE)	**557%**
3. 80A Resin	**340%**
4. Fluoroacrylate	**338%**

(c)

2.1.10 SHPo Drag Reduction on Racing Vessels

SHPo technology also has an opportunity to make its debut into the market on a smaller scale. In competitive boat races, known as regattas, a few seconds difference may decide victory from defeat, and the drag reduction offered by SHPo surfaces could position itself as a decisive factor. Olympic regattas (rowing and sailing) typically have guidelines preventing unorthodox or excessive modifications of the boats, meaning SHPo technology would need to fight an uphill battle to appeal to policy makers [114], [115]. Competitive regattas outside of the Olympics, such as powerboat, hydroplane, and yacht racing, typically have more lenient restrictions against hull modifications and could be an entry point for SHPo technology [116]. In 1987, 3M collaborated with the U.S. yacht racing team to coat the bottom of the Stars & Stripes racing yacht with a micro-structured, drag-reducing riblet film that helped the team to win the America's Cup yacht race [117]. 3M experimented with their drag-reduction riblet film again in 2010, partnering with BMW Oracle Racing to coat a racing vessel with riblet film in the 33rd America's Cup [118]. Unfortunately, riblet film or any performance-enhancing technology has since been banned in the Americas Cup [115]. Nevertheless, the use of riblet film to help the Stars & Stripes and BMW

Oracle Racing achieve victory shows that drag reducing films can be a useful tool for significantly increasing the speeds of watercraft.

Cigarette boats, part of the powerboat racing family, cost roughly $500,000 for a typical 42 ft-long boat [119]-[121]. With a length of 42 ft, beam of 8 ft, and draft of 3 ft, the approximate wetted surface area of the cigarette boat, using Equation 2.1, is 460 ft^2 [122]. The dry-docking cost for recreational boats is less expensive than that of cargo ships. It is approximated that the dry-docking cost is $5.00 per foot per day, or $210 per day for the 42 ft cigarette boat [123]. It is estimated that two experienced film wrappers could finish the job in one day, based on the experience of a drag-reducing boat film called Finsulate, which is also applied to the hull as an adhesive-backed film in a similar method to how SHPo surfaces are expected to be applied [124]. Hence, it is approximated that the cost of applying SHPo surfaces to the cigarette boat is roughly $6,000 to $8,000 depending on the substrate material used, as summarized in Table 2.3. This means the cost of applying SHPo surfaces to the cigarette boat is roughly 1.5% of the total cost of the boat.

Table 2.3: Cost estimates for a 42 ft-long cigarette boat, assuming the trench SHPo surfaces are applied to a wetted surface area of 460 ft^2 (or 43 m^2) and fabricated using either fluoroacrylate, PDMS, PTFE, or 80A Resin. (a) Cost of goods and (b) Product cost.

	Unit Price	Quantity	Total Cost
Installation Costs			
Installer Wages	$30.00 /hour	48 manhours	$1,440
Dry Docking	$210 /day	1 days	$210
Material Costs			
Substrate Material Options			
1. PDMS	$69.18 /gal	4 gal	$242
2. Teflon (PTFE)	$75.92 /gal	4 gal	$266
3. 80A Resin	$527.31 /gal	4 gal	$1847
4. Fluoroacrylate	$532.71 /gal	4 gal	$1866
Backing film & liner	$32.27 /m²	43 m²	$1385
Acrylic adhesive	$111.18 /gal	1.4 gal	$159
Manufacturing Costs			
Manufacturer Wages	$60.00 /hour	2 manhours	$143
Machine Operating Costs	$17.20 /hour	0.5 hours	$8
Cost of Goods Sold			
COG of Each Material Choice			
1. PDMS			**$3,588**
2. Teflon (PTFE)			**$3,611**
3. 80A Resin			**$5,192**
4. Fluoroacrylate			**$5,211**

(a)

	Total Amount
Total Commercial Product Cost	
Gross Profit Margin	30.68%
Sales Tax	10.00%
Investment Cost (Price for Consumer) of Each Material Choice	
1. PDMS	**$5,693**
2. Teflon (PTFE)	**$5,730**
3. 80A Resin	**$8,239**
4. Fluoroacrylate	**$8,269**

(b)

The drag reduction of SHPo surfaces will increase the top speed of the vessel because they will reduce the hull's coefficient of drag C_D. The relationship between C_D and hull speed U is shown in Equation 2.4, where ρ is fluid density, A is wetted surface area, and D is drag force.

$$D = \frac{1}{2}\rho A U^2 C_D \tag{2.4}$$

As mentioned before, SHPo surfaces have been reported to offer 30% skin friction drag reduction in a real-world marine environment [52]. The shape of cigarette boat hulls is simpler and more easily covered with SHPo surfaces than the complex hulls of cargo ships. SHPo surfaces will likely be coated on roughly 80% of the wetted surface of the planing boat, so it is estimated that overall drag reduction will be roughly 25% in practice. A paper from Korea Institute of Ocean Science & Technology and Seoul National University studied planing vessels with V-shaped hulls in a towing tank. Their measured results showed that skin friction drag accounts for roughly 50%–70% of the total drag on planing vessels travelling at high speeds (faster than 45 knots) [125]. Hence, it is approximated that the application of SHPo surfaces onto a V-shaped cigarette boat can reduce C_D by 12.5%. Using a free body diagram of the forces acting on the planing boat, shown in Figure 2.5, it is assumed that the thrust force T and drag force D are related via Equation 2.5.

$$D = T\cos(\alpha) \tag{2.5}$$

It is assumed that thrust T of the speedboat's motor at full throttle is constant and will be the same before and after SHPo surfaces are applied to the vessel. It is also assumed that the changes in trim angle α and wetted surface A are negligible before and after SHPo surfaces are applied and the vessel's top speed increases. Following these assumptions, the total drag force D experienced by

the speedboat is the same before and after the SHPo surfaces are applied. The percent increase of the vessel's top speed is derived in Equation 2.6

$$
\begin{aligned}
D_o &= D_f \\
\rho_o &= \rho_f \\
A_o &= A_f \\
C_{D,f} &= 87.5\% \times C_{D,o} \\
\frac{D_f}{D_o} &\propto \frac{\frac{1}{2}\rho_f A_f U_f{}^2 C_{D,f}}{\frac{1}{2}\rho_o A_o U_o{}^2 C_{D,o}} \\
\frac{U_f}{U_o} &\propto \sqrt{\frac{C_{D,o}}{C_{D,f}}} = 1.07
\end{aligned}
\tag{2.6}
$$

where D_o, ρ_o, A_o, U_o, and $C_{D,o}$ are the drag force, fluid density, wetted area, speed, and coefficient of drag all before SHPo surfaces are applied, respectively. Similarly, D_f, ρ_f, A_f, U_f, and $C_{D,f}$ are the drag force, fluid density, wetted area, speed, and coefficient of drag all after SHPo surfaces are applied, respectively. Hence, applying SHPo films to the cigarette boat's hull offers an estimated 7% increase in top speed while costing only roughly 1.5% of the total cost of the boat as estimated above.

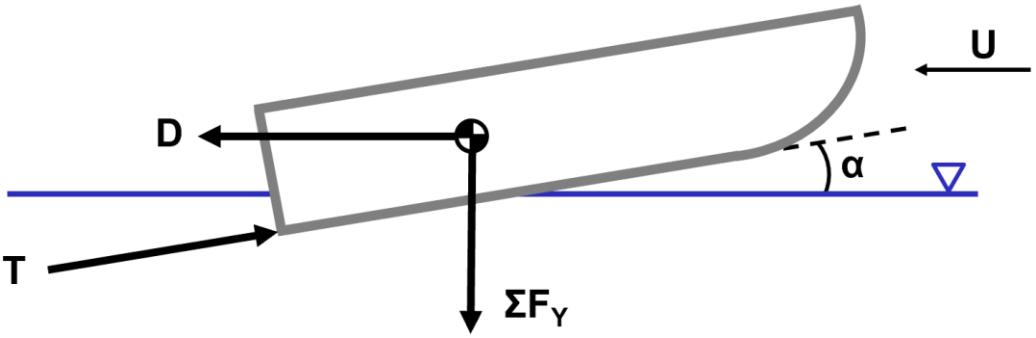

Figure 2.5: Free body diagram of a planing vessel, using the information in [126]. *T* is thrust force, *D* is drag force, α is trim angle, and ΣF_Y is the sum of the vertical forces, composed of the hydrodynamic lift force and the weight force. *U* is the velocity of the boat. The hull of the boat is shown in gray lines, and the free surface of water is shown in a blue line.

2.2 Existing Products Competing with SHPo Drag Reduction

2.2.1 Copper Antifouling Coatings

The most common technique of reducing drag on marine vessels is anti-fouling coating. This is since biofouling, such as barnacles and algae, commonly attach to boat hulls. The biofouling increases the weight of the vessel and adversely affects the hydrodynamic performance of the hull, causing a drag increase of up to 60% [127]. Anti-fouling products function by coating the wetted surface area of the boat hull with a material that inhibits the organisms' ability to attach to the hull surface. The most popular type of anti-fouling coating is the copper-based ablative coating [128]. Copper-based ablative coatings create a layer of toxic copper paint on the wetted surface area of the hull, poisoning biofouling that tries to attach to the hull [129]. The copper paint also gradually peels away in the water, causing any stubborn biofouling attached to the hull to lose

its grip and float away. The peeling anti-fouling paint reveals another layer of toxic paint beneath it, until the paint runs out and must be replaced via re-painting. The longevity of the copper paint is roughly two to three years [130]. The primary concern with copper-based ablative coatings is that the biocide is leaked off the boat's hull and into the seawater at rates as high as 25−65 μg of Cu per cm^2 per day, poisoning the natural marine environment [131]. The Suez Bay transit area sees 35 tons of copper polluted into its seawater every year due to antifouling marine coatings, accounting for 83% of the total copper polluted into the Suez Bay [87]. This causes certain areas of the Suez Bay to exceed the safe limit of copper levels, which is 3.1 μg of dissolved copper per liter of seawater [87]. Research by the United States environmental protection agency has found copper levels as high as 8.0 μg/L in San Diego Bay and 29.0 μg/L in Newport Bay [87]. While non-copper antifouling paints exist, it has been found that some non-copper alternatives might also be just as harmful as the copper paints [128]. SHPo surfaces show promise of having non-toxic anti-fouling properties, which would mean that SHPo technology could become an environmentally friendly alternative to copper antifouling coatings [5].

2.2.2 Non-Toxic Antifouling Paint

Due to the harm that copper-based paints pose to the environment, non-toxic antifouling paints are being studied and developed [87], [128], [131]. The operating principle of non-toxic antifouling paints is that the chemical composition of the paint reduces the adhesion strength of the biofouling, causing them to have a weak grip to the hull's surface and ultimately detach from the hull without harm [132], [133]. Non-toxic alternatives include paints fabricated with silicone, fluoropolymer, epoxy, or Teflon (PTFE) [128], [134]-[136]. However, of the non-toxic

alternatives developed thus far, some studies claim that silicone-based paint is the only option that is effective enough to compete with toxic antifouling paints [133], [134]. A popular non-toxic paint brand, named Intersleek, makes antifouling paint products composed of silicone or fluoropolymer [137]. Intersleek has already been applied in over 5000 marine applications since its creation in 1996, displaying the potential for non-toxic alternative paints to supplement copper-based paints. [137]. Certain paints using fluoropolymer-modified silicone nanocomposites, such as Intersleek, claim to combine the antifouling properties of both hydrophilic and hydrophobic surfaces to enhance their antifouling effectiveness, dubbing themselves as amphiphilic [133], [137]. However, most silicone-based paints gradually dissolve silicone into the marine environment over time [128], [134], [138]. While the silicone is not considered a biocide, the leaching of this chemical into the seawater casts uncertainty over the claims that the paint is truly ecologically friendly [138]. To counter this, the company SeaCoat has created the first hard silicone-based antifouling paint, called SeaSpeed [139], [140]. The extremely hard surface of SeaSpeed's chemistry prevents the silicone from seeping into the environment [139], [140]. Nevertheless, studies have found that silicone-based paint is only partially effective against biofouling, since it is susceptible to the adhesion of biofilm and most effective only against larger bio-organisms [134], [135].

2.2.3 Antifouling with Finsulate

Much like how SHPo surfaces hope to become an eco-friendly alternative to toxic ablative coatings, a product called Finsulate prevents biofouling in a unique way. Finsulate mimics the design of sea urchin spines to make it difficult for biofouling to attach to the hull's surface [141]. The Finsulate product is an adhesive film that is applied to the wetted surface area of the boat hull,

in which the film has been coated with nylon fibers that are 3 mm long, 50 μm thick, and have a density of 40 fibers/mm^2 [142]. A schematic describing the Finsulate film is shown in Figure 2.6. Finsulate film is fabricated using roll-to-roll manufacturing. Specifically, Finsulate uses the method of electrostatic flocking to adhere the nylon fibers to the adhesive-backed film [142]. The electrostatic flocking manufacturing process is described in Figure 2.7.

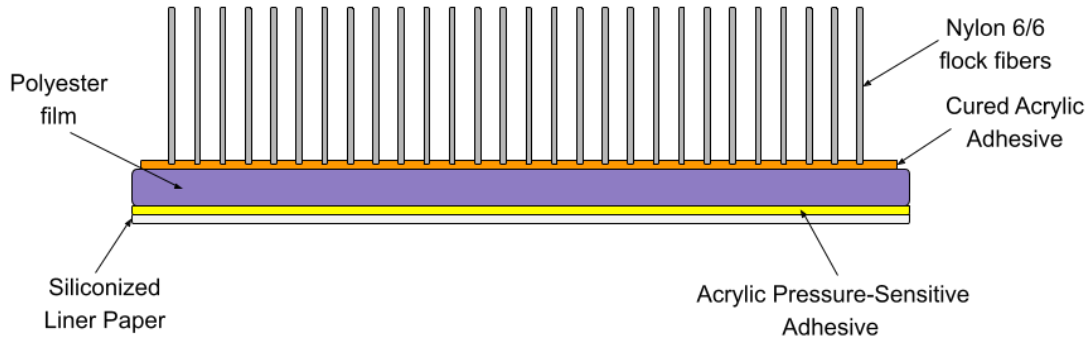

(a)

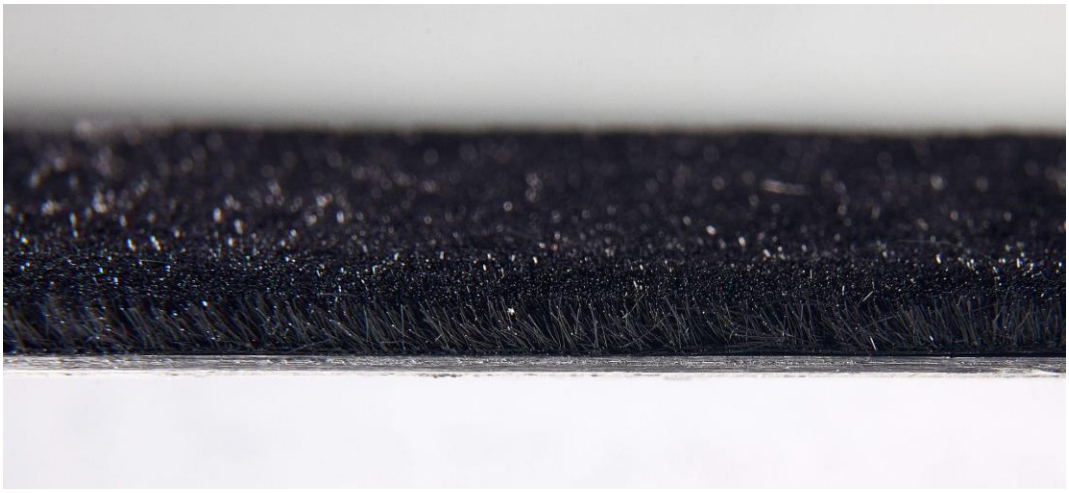

(b)

(c) 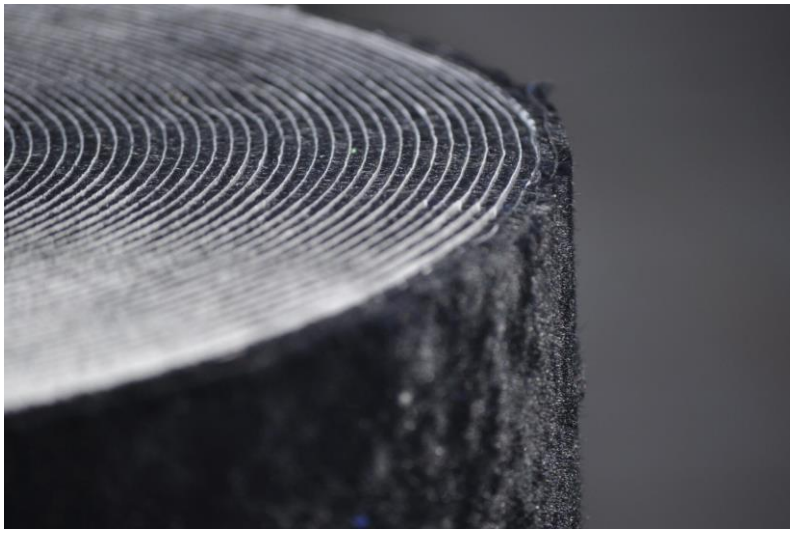

Figure 2.6: (a) 2D diagram describing the Finsulate film, based on Finsulate's patent information [142]. (b) Side view close-up image of the Finsulate film. (c) Finsulate wrapped film. Figure 2.6b duplicated from [143]. Figure 2.6c duplicated from [144].

(a) 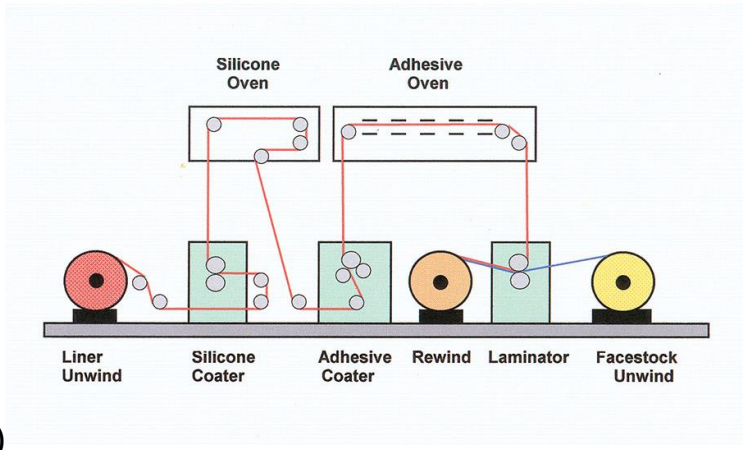

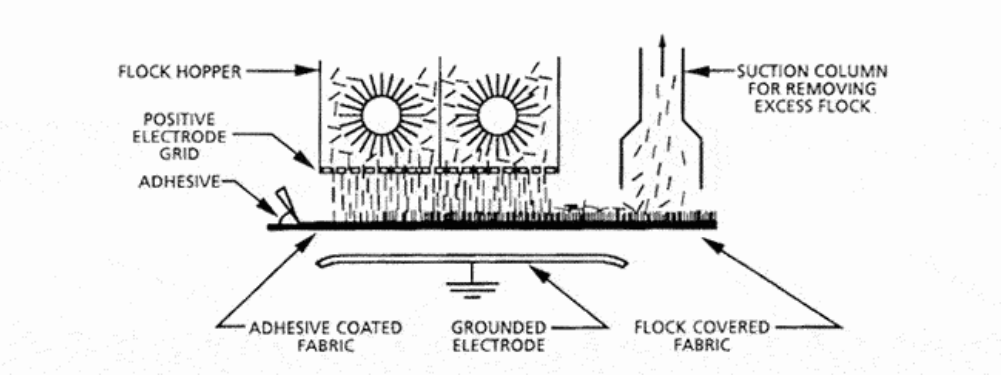

(b)

Figure 2.7: (a) Diagram portraying how R2R manufacturing fabricates an adhesive-backed film. (b) Method in which electrostatic flocking adheres the fibers, also called flock, to the film. Figure 2.7a duplicated from [145]. Figure 2.7b duplicated from [146].

The founder of Finsulate, Rik Breur, estimates that the cost of applying Finsulate wrap to a typical 40 ft boat would be €3,000, which is comparable to the estimated cost of applying SHPo surfaces to a 40 ft boat (see Table 2.3) [147]. The commercial success of Finsulate shows promise for the adoption of SHPo surfaces into the market of boat coatings. Finsulate's successful use of R2R manufacturing to fabricate their product also shows that it is feasible that a similar manufacturing method could be used to mass-produce SHPo surfaces. Micro-trenched SHPo surfaces also hold an advantage over the Finsulate product. Finsulate prevents the form drag that a boat would experience if it were to be covered in biofouling. However, when studying the effect of Finsulate on a high-speed planing vessel with no biofouling, it was found that Finsulate's 3 mm fibers caused a 20% decrease in max speed due to increased skin-friction drag caused by the fibers [147]. Finsulate does offer a 1 mm-long-fiber variant of Finsulate film for high-speed planing vessels, which only decreases the top speed by 1%, but has slightly less effective biofouling

prevention [144], [147]. However, Finsulate does not offer any overall drag reduction aside from preventing drag from biofouling that would otherwise be attached to the hull. SHPo surfaces, on the other hand, may not only prevent the drag that would be caused by biofouling, but also inherently reduce the friction drag on the hull by 30% due to its micro-structures [52]. Hence, SHPo surfaces are positioned to become a more effective drag-reducing product than Finsulate.

Chapter 3: Development of Model Boats to Test Drag Reduction with Small Samples of Film

3.1 Model Boat Testing Procedure

3.1.1 Motivation

This thesis aims to create a testing procedure to rapidly and conveniently test the drag reduction caused by small (several centimeters) surface samples in turbulent open-water conditions. This procedure will be used to test samples of flexible SHPo film that will be fabricated by the UCLA Micro & Nano Manufacturing Laboratory in the future. The current manufacturing methods used by the UCLA Micro & Nano Manufacturing Laboratory to fabricate the SHPo film samples have a low throughput. Hence, the size of the boat used in this study must be relatively small, such that only several samples are needed to cover a significant portion of a boat hull's wetted surface area. However, the boat should be large and fast enough to reach fully turbulent flows, which the previous small boat studies failed to achieve [62]-[64]. Covering a large portion of the hull with SHPo samples will affect the bulk hydrodynamic performance of the vessel, which is something that has not been extensively studied in the literature yet. The testing procedure must be convenient so that newly developed SHPo samples can be tested without requiring excessive amounts of time and money. Should the SHPo samples show promise of beneficial drag reduction, the samples will be tested further in a procedure developed at UCLA that utilizes a shear comparator mounted underneath a passenger motorboat [52]. In the model boat procedure of this paper, the presence of beneficial (positive) SHPo drag reduction is tested by comparing a model boat that is outfitted with SHPo samples to an identical model boat outfitted with smooth samples. If the boat with SHPo samples travels at a higher top speed during steady planing than the boat

with smooth samples, it is inferred that the SHPo samples produce positive drag reduction. The fabrication and testing of newly developed SHPo samples is left to future studies; this paper simply establishes the testing procedure and demonstrates that the identical model boats travel at the same steady speed.

3.1.2 Fabricating Testing Boats

Remote-controlled (RC) boats are chosen as the vessels upon which to test the SHPo samples in this experimental procedure. RC boats fit the size and convenience requirements and allow testing to take place in natural, open-water conditions. The tests are performed at Lake Balboa in the San Fernando Valley, which is the closest natural body of water to UCLA that welcomes RC boating. Tests are performed early in the morning when wind speed is low, and the lake water is effectively stagnant. The model of RC boat used in this study is the Pro Boat Blackjack 24” catamaran RC boat, shown in Figure 3.1.

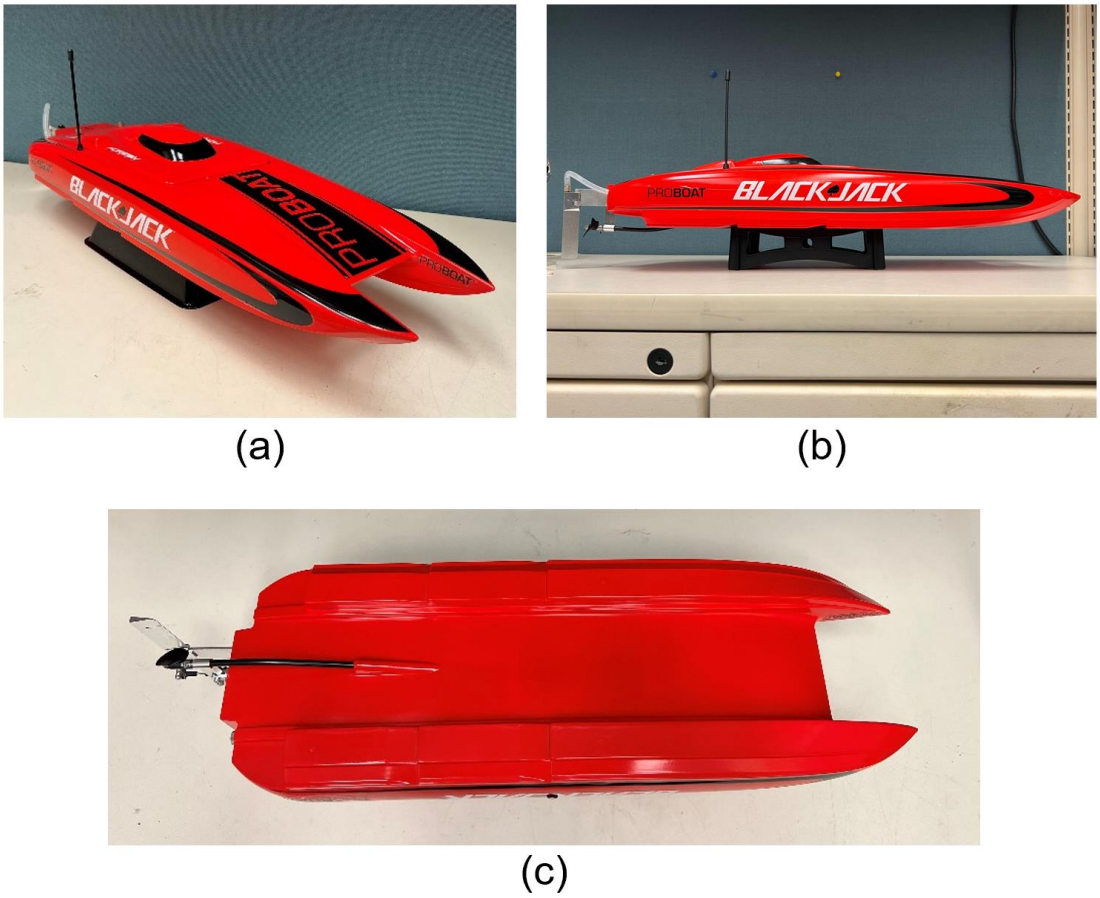

Figure 3.1: Pro Boat Blackjack 24” RC boat before modifications from the (a) isometric view, (b) side view, and (c) bottom view.

It is important that when surface samples are attached to the model boat, the outer surfaces of the samples are flush with the outer surface of the hull. Otherwise, a pressure drag would be generated by the samples’ side edges that face the oncoming flow. This would interfere with the boundary layer across the samples and adversely affect the hydrodynamic performance of the hull. To allow for the samples to be adhered in a manner that makes them flush with the outer surface of the hull, a holder plate is designed using CAD software and fabricated via 3D-printing. The

holder plate possesses a recess in which to hold the samples, as shown in Figure 3.2. To accommodate for the small size of the build plate of the 3D printer, the holder plate is manufactured in three separate components with aligner features that ensure that the components are flush when they are fit together. The holder plate components are adhered to each other and to the RC boat hull with epoxy resin. The front of the holder plate has curved geometry that matches the curve of the front of the model boat's hull. This was achieved by importing a side-view image of the model boat into CAD software and using splines to trace the image, as shown in Figure 3.3.

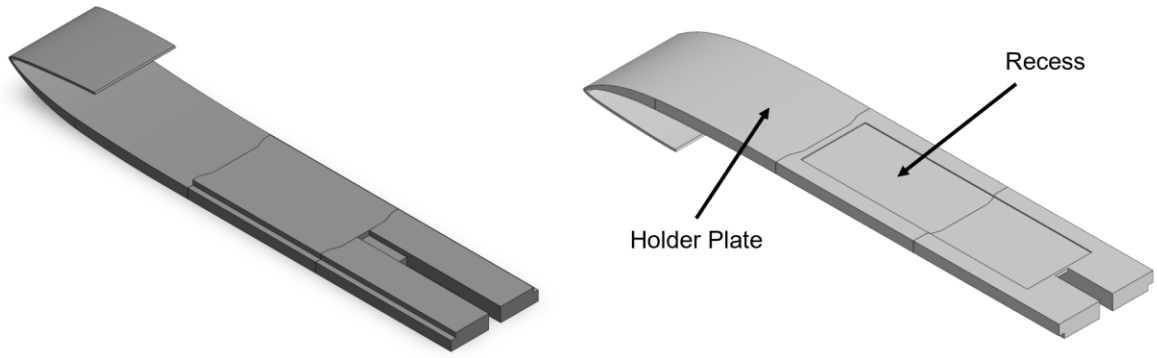

(a) (b)

(c) (d)

Figure 3.2: CAD model of holder plate showing isometric views looking at (a) the top surface of the plate and (b) the bottom surface of the plate with the recess. Images of the finished, 3D-printed holder plate are also shown in isometric views looking at the (c) top surface and (d) bottom surface.

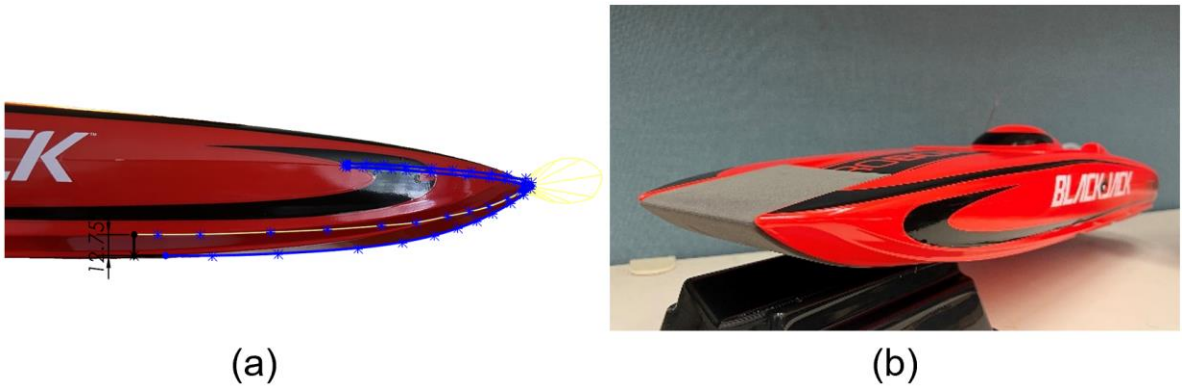

Figure 3.3: (a) Splines in CAD software mapping the curve of the front of the model boat's hull. (b) 3D-printed plate matching the curve of the RC boat hull.

Samples are adhered to the holder plate using double-sided PET tape, so that the samples can be removed and replaced after an experiment. This allows the testing procedure to be repeated with newly developed samples that have different features, such as different micro-structure pitches, gas fractions, a new substrate material, or a new manufacturing method. It is assumed that the SHPo surfaces made in the future will be 1 mm thick. The recess in the center of the holder plate is designed so that the top surfaces of the attached samples are flush with the outer-facing surface of the plate, accounting for the 1 mm thickness of the samples and the 0.14 mm thickness

of the adhesive tape. The recess holds eight 4 cm by 7 cm samples, in the manner illustrated in Figure 3.4.

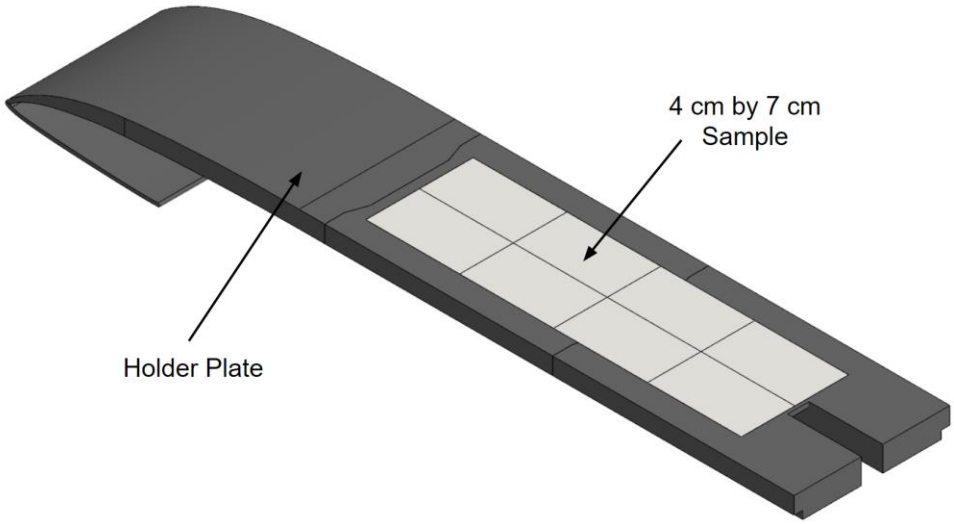

Figure 3.4: CAD model of holder plate with eight 4 cm by 7 cm samples inserted into its recess.

The holder plate components are fabricated with Nylon 12 powder using a Formlabs Fuse 1 selective laser sintering (SLS) 3D printer at the UCLA Lux Lab. SLS printing was chosen because of its high part resolution and accuracy. When prototypes were made of ABS or PLA material using a Prusa i3 MK3S fused deposition modeling (FDM) 3D printer at the UCLA Makerspace, the resulting printed parts were slightly warped, causing misalignment and exposed gaps when the parts were attached to the model boat's hull, as shown in Figure 3.5. Fused Nylon 12 material possesses a water absorption coefficient of 0.66%, and exposure to water for one hour would lead to a weight gain of 0.1% [148]. If the holder plates were to absorb water, it would inhibit the adhesion of the double-sided tape securing the samples to the boat. To seal the outer layer of the Nylon 12 components and prevent any water absorption, the Nylon 12 plates are

sprayed with Rustoleum NeverWet, as shown in Figure 3.6. The recess of the holder plate is not sprayed with NeverWet, since the NeverWet coating would inhibit the ability of the double-sided tape to adhere to the recess's surface.

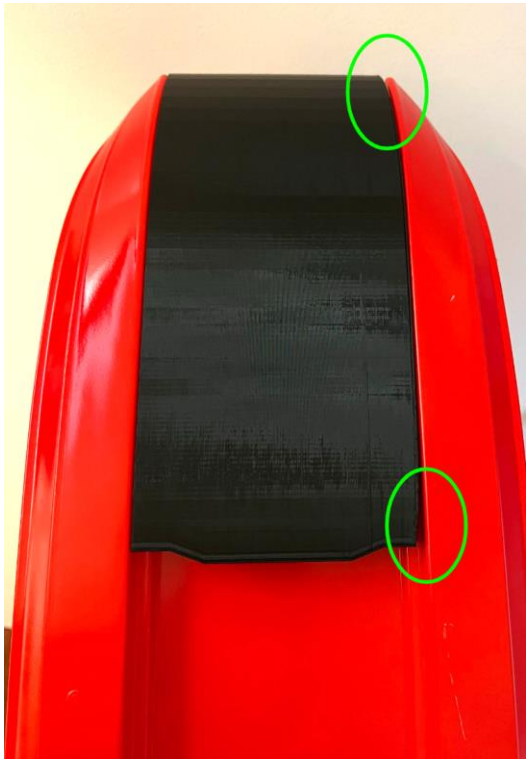

Figure 3.5: When printing the holder plate components using FDM 3D-printing, the warped shape of the component exposes gaps in the new hull design, as highlighted by the green circles. Hence, the high resolution of SLS printing needed to be used instead.

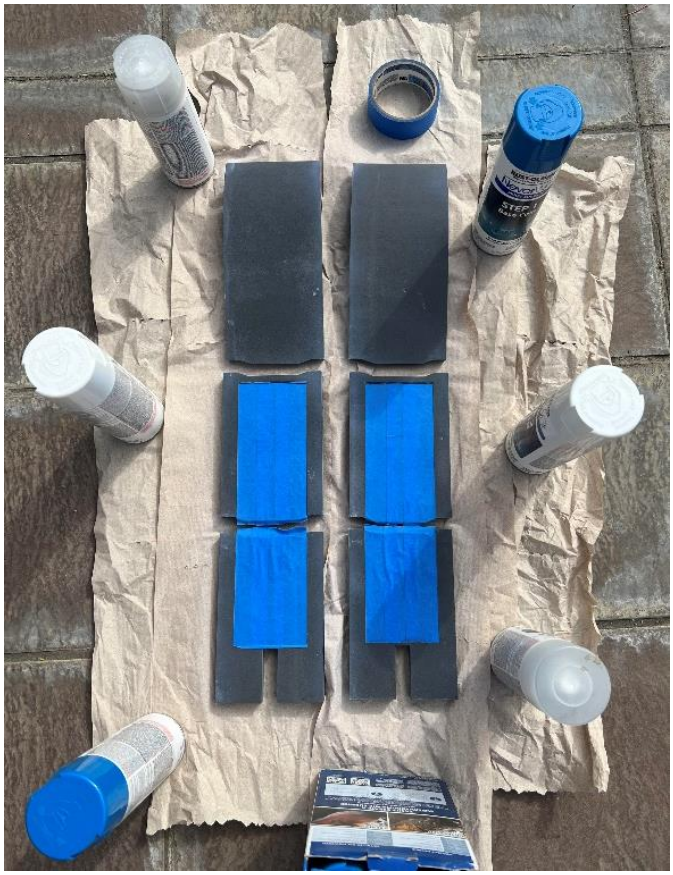

Figure 3.6: Spray-coating the Nylon 12 holder plates with NeverWet spray. The recess of the holder plate is covered so that it is not coated with NeverWet.

The holder plate components are adhered to each other and to the RC boat hull with epoxy resin. The Part 1 and Part 2 components of the epoxy are mixed in a ratio that is predetermined by the manufacturer, and the ratio is properly dispensed by one single pump of each epoxy container. Approximately 1 gram of adhesive filler is added to the epoxy resin during its pot life to improve the adhesion properties of the resin once it cures. The three components of the epoxy resin are shown in Figure 3.7. The components of the holder plate are adhered inside the gap of the catamaran hull of the RC boat using the epoxy resin, as illustrated in Figure 3.8. Note that as a

consequence of this modification, the boat is converted from a catamaran hull to a flat monohull. Once the epoxy resin cures, the gaps between the edges of the holder plate components and the RC boat hull are filled with 3M marine-grade sealant to protect the epoxy resin from eroding over time from contact with water. This is achieved by covering the surface of the hull with masking tape, exposing only the gaps between the hull and the holder plate. Then 3M marine-grade sealant is applied to the hull and pressed into the gaps with a painting knife. The process of applying the marine sealant to the boats is displayed in Figure 3.9. When the SHPo surfaces to be tested are fabricated in the future, and the recess would be covered with these samples, preventing water from contacting the recess's surface. The boat without SHPo surfaces will have mock-up non-SHPo smooth samples placed in the recess, which have the same dimensions as the SHPo surfaces but not have drag reduction effects. For now, the recess is water-proofed by covering its surface with the double-sided tape and leaving the tape's outer-facing plastic liner attached, as shown in Figure 3.10.

Figure 3.7: The Part 1, Part 2, and Adhesive Filler components of the epoxy resin.

Figure 3.8: The RC boats with holder plates attached are shown from the (a) front view and (b) back view. The plates are adhered to the hull with epoxy resin.

Figure 3.9: 3M marine-grade sealant is applied to the small gaps between the edges of the plate components and the hull. (a) Masking tape is used to cover the surface of the hull, exposing only the gaps. Then, sealant is coated atop the surface and spread into the gaps. (b) Once the sealant has cured, the tape is removed, leaving only the sealant that has cured inside the gaps.

Figure 3.10: The double-sided tape with its orange plastic liner covers the recess, preventing water from permeating into the surface of the uncoated portion of the Nylon 12 sample holder plate.

The RC boats are driven by a water-cooled 2000 Kv brushless motor and 30 A LiPo-compatible electronic speed controller (ESC). The boats are each powered by a single 5200 mAh 80C 3-S battery, which delivers 12.6 V to the motor at full charge. As a LiPo battery discharges, the amount of supplied voltage gradually decreases [149]. To ensure that both boats are powered at the same voltage level, the 3-S batteries are fully charged to 12.6 V with a smart charger before testing and replaced with a new fully charged battery after only a couple runs. The boats are controlled by the Spektrum STX 2.4 GHz FHSS radio system that consists of a handheld pistol-

grip transmitter and an on-board receiver that is connected to the ESC. The electronic components that drive the RC boats are shown in Figure 3.11.

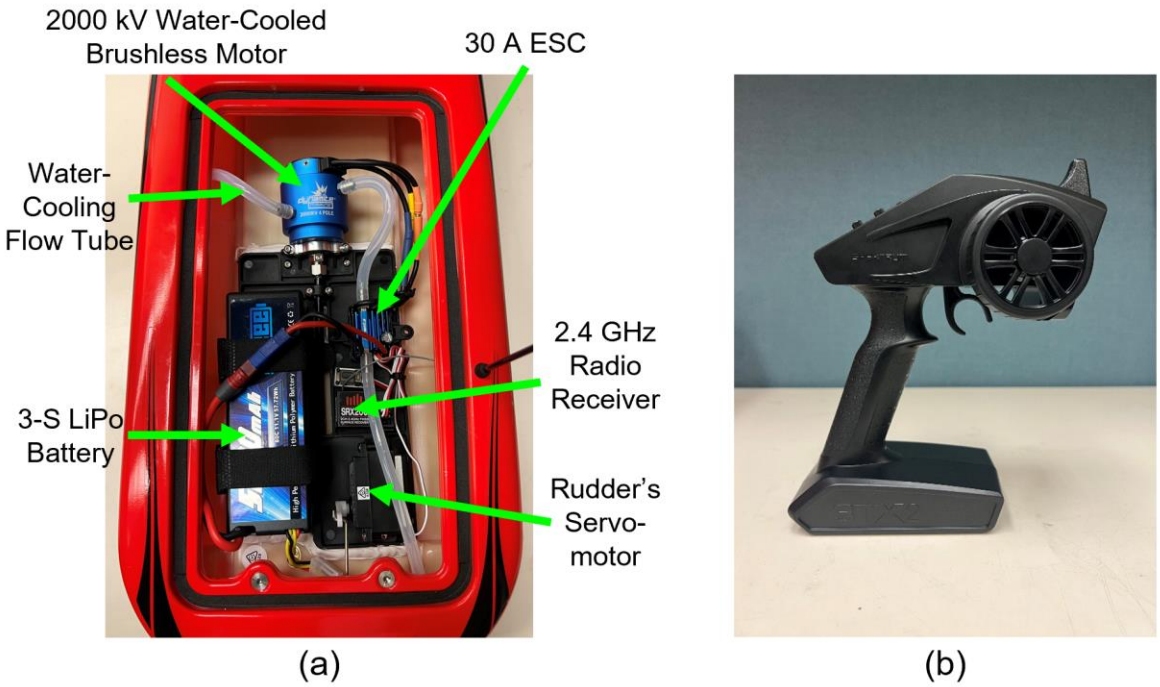

Figure 3.11: Electronic components of the RC boat, where (a) shows the components on-board the boat and (b) shows the handheld pistol grip transmitter.

The speed of each of the model boats is measured by a SkyRC GSM-015 GPS speedometer. The GPS device records latitude, longitude, altitude, and timestamps at a refresh rate of 1 Hz. Boat speed is calculated between datapoints by converting the latitude, longitude, and altitude data to cartesian vector coordinates. It is assumed that the earth is shaped as a perfect sphere, so the dot product and arc length equations can be used to calculate distance traveled between the vector coordinates. Speed is calculated by dividing the distance traveled by the time between the two data

points. These calculations are automated with a MATLAB script that is converted into a Microsoft Excel add-in. The GPS speedometers are put into a sealed plastic bags for waterproofing and taped to the roof of each of the RC boat's cabins, as shown in Figure 3.12.

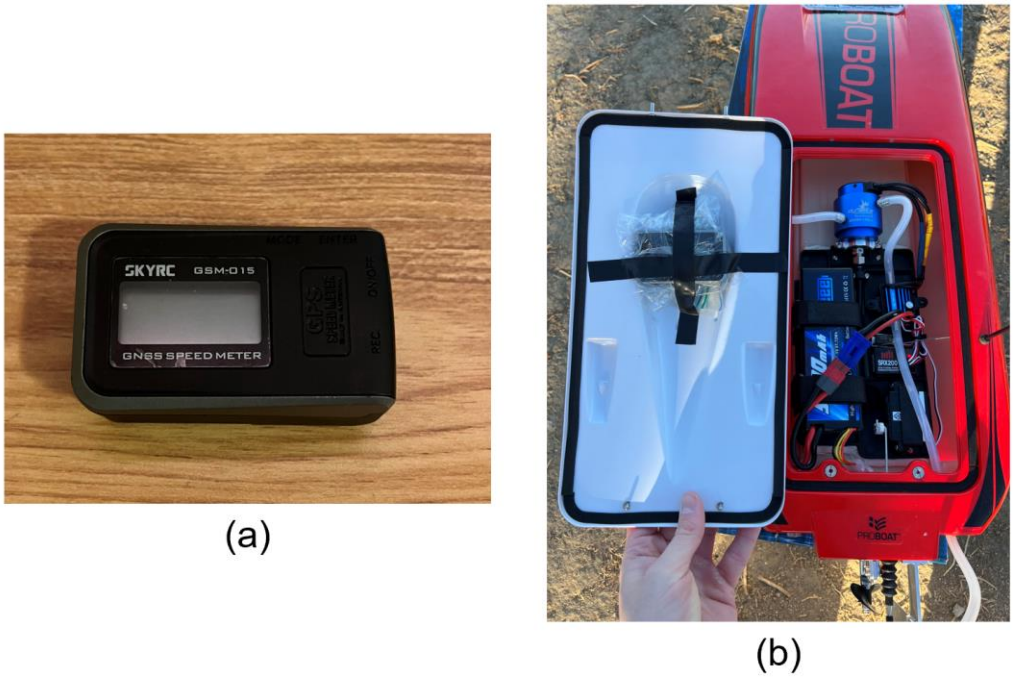

Figure 3.12: (a) The SkyRC GSM-015 speedometer. (b) GPS speedometers are secured to the roof of each of the RC boats to measure speed data during the test trials.

GPS devices possess error due to several factors [150]. Error may be caused because the GPS satellites' position and time data sent to the speedometer may have errors itself. The signal sent to the speedometer is also delayed as it experiences refraction when passing through the earth's atmosphere. The GPS signal experiences multi-path interference error if the signal is obstructed by objects around the GPS speedometer, such as tall buildings or trees. Error may also be caused by electronics errors inside the GPS speedometer itself. To calculate the error of the

GPS devices used in this paper, the speedometers were placed in an open area of Lake Balboa and left stationary for one hour. Despite being left untouched for one hour, each of the GPS devices measured a peak speed of 0.164 m/s. Hence, the speed data of the GPS speedometer has an error of ±0.2 m/s.

3.1.3 Proving Drag Reduction with Differential Velocities

The existence of beneficial drag reduction is proven by comparing the velocity of the model boat with SHPo samples to the velocity of the identical RC boat with smooth samples. The samples are applied to fill the recess made on the hull surface of the boat. To measure comparable velocities, the boats must have equal thrusts. Hence, the boats are driven with the same motors, ESCs, batteries, and throttle settings. The tests must also be performed in the same ambient wind, water flow, and temperature conditions. To ensure that these conditions are met, the two model boats are run one after the other when recording speed data.

By studying the free body diagrams of a boat in motion, it can be shown that if the boat with SHPo samples travels at a faster top speed than the boat with smooth samples, it can be inferred that the SHPo samples cause beneficial drag reduction. The drag reduction of SHPo surfaces affect the model boat's speed because they change the hull's coefficient of drag C_D. The relationship between C_D, hull speed U, and drag force D was given in Equation 2.4. If the test boats are traveling at a speed that is slow enough relative to the wetted length of their hull, such that the wavelength of the transverse waves generated by the vessel are shorter than the vessel's wetted length, then the boat acts as a displacement hull [151], [152]. A displacement hull is held up by

buoyancy, as illustrated in the free body diagram shown in Figure 3.13. Here F_B is buoyancy force, D is drag force, T is thrust force, F_g is the weight force, and U is the relative velocity of the water. The speed data that will be analyzed occurs when the boats are traveling steadily at constant velocities, so the net force is zero. As can be deduced from Figure 3.13, the horizontal force balance implies that the drag force D and thrust force T must be equal, as shown in Equation 3.1.

$$D = T \tag{3.1}$$

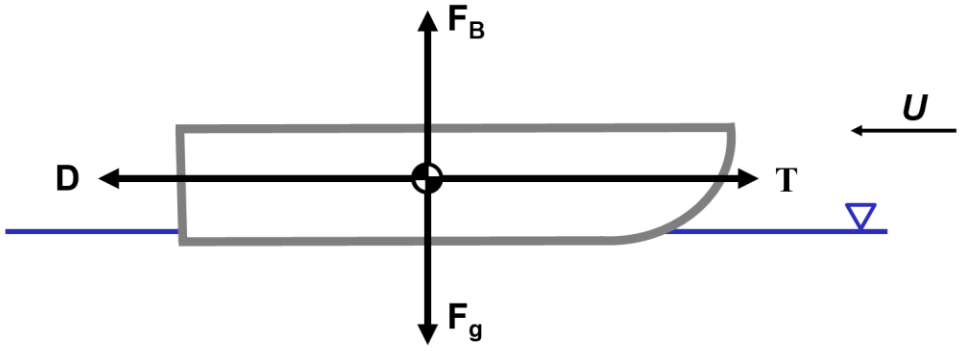

Figure 3.13: Free body diagram of a displacement-hull boat. T is thrust force, D is drag force, F_B is buoyancy force, and F_g is weight force. U is the velocity of the boat. The hull of the boat is shown in gray lines, and the free surface of water is shown in blue lines.

However, the model boats must travel at high-speed to achieve a Reynolds Number of $Re_x > 3\times10^6$ and experience fully turbulent flow conditions [153]. At high speed, the model boats act as planing hulls rather than displacement hulls. A boat acts as a planing hull if it is traveling at a fast enough speed such that the wavelength of the generated transverse waves is larger than the

boat's wetted length, which causes the boat to rise above the crest of its bow wave [151], [152]. A planing hull glides on top of the water and is held up by the lift created by its thrust force. Refer to Figure 2.5 for the free body diagram of a planing boat, and Equation 2.5 for the horizontal force balance of the planing hull. It is assumed that the trim angle α and wetted surface area A change by a negligible amount when the boat is steadily planing at a certain speed compared to another. Based on the assumptions made, Equations 2.5 and 3.1 show that if the two model boats have the same thrust, they also have the same drag, assuming both boats are planing or both are acting as displacement hulls. If both model boats have the same D, ρ, and A, then Equation 2.4 infers that the ratio of the speeds of the boats is directly proportional to the square root of the ratio of the drag coefficients of the boats' hulls, where the difference in drag coefficients is caused by the SHPo surfaces, as was shown in Equation 2.6.

3.1.4 Using Dual-Rate Adjustments to Set the Throttle Limit

In case the two RC boats are not truly identical, due to discrepancies during manufacturing and drifts over time, the dual-rate throttle adjustments of each boat's RC transmitter may be fine-tuned to ensure equal thrust. Dual rate throttle adjustment scales the range of the possible throttle inputs, so that the maximum throttle value can be adjusted. Hence, the transmitters can be tuned such that applying maximum throttle input on the handheld pistol grips of each boat results in the same amount of thrust being applied to both boats during a test. The model boats used in this thesis did not have noticeable discrepancies when measuring their top speed, so the dual-rate throttle adjustment knob of each boat was left at 100%. The remotes also possess a throttle limiter switch that performs the same function as the throttle adjustment knob, but with digital settings instead

of analog settings. Speed tests were performed when the throttle limiter switch was set to 75% and to 100%, to study the boat at low speed and high speed. The handheld transmitter is shown in Figure 3.14.

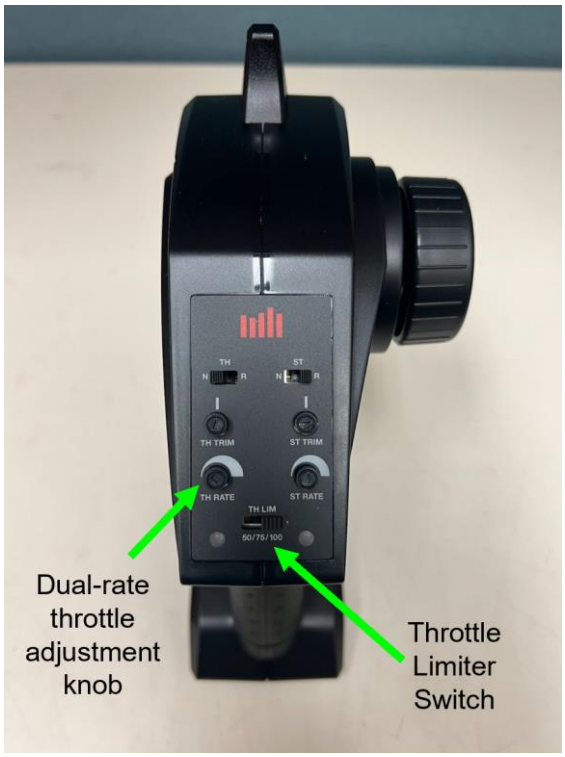

Figure 3.14: Top view of the handheld pistol-grip RC transmitter, showing the dual rate throttle adjustment knob and the throttle limiter switch.

3.2 Discussion of Results

Before SHPo samples can be studied with this experimental procedure, it must be proven that the two boats reliably travel at the same speed when the boats are traveling steadily with equal throttle inputs. To prove this, the two model boats created for this procedure are taken to Lake

Balboa and their speeds are measured for equal throttle inputs. During each test run, the triggers of the pistol grip transmitters are squeezed fully, the dual-rate throttle adjustment knobs are set to 100%, and the throttle limiter switches are set to the same setting. Tests are performed when both the throttle limiter switches are set to 75% and when they are set to 100%. At 75% throttle limit, the RC boats did not move fast enough to begin planing, so they traveled as displacement hulls. The results of the displacement hull tests are shown in Figure 3.15.

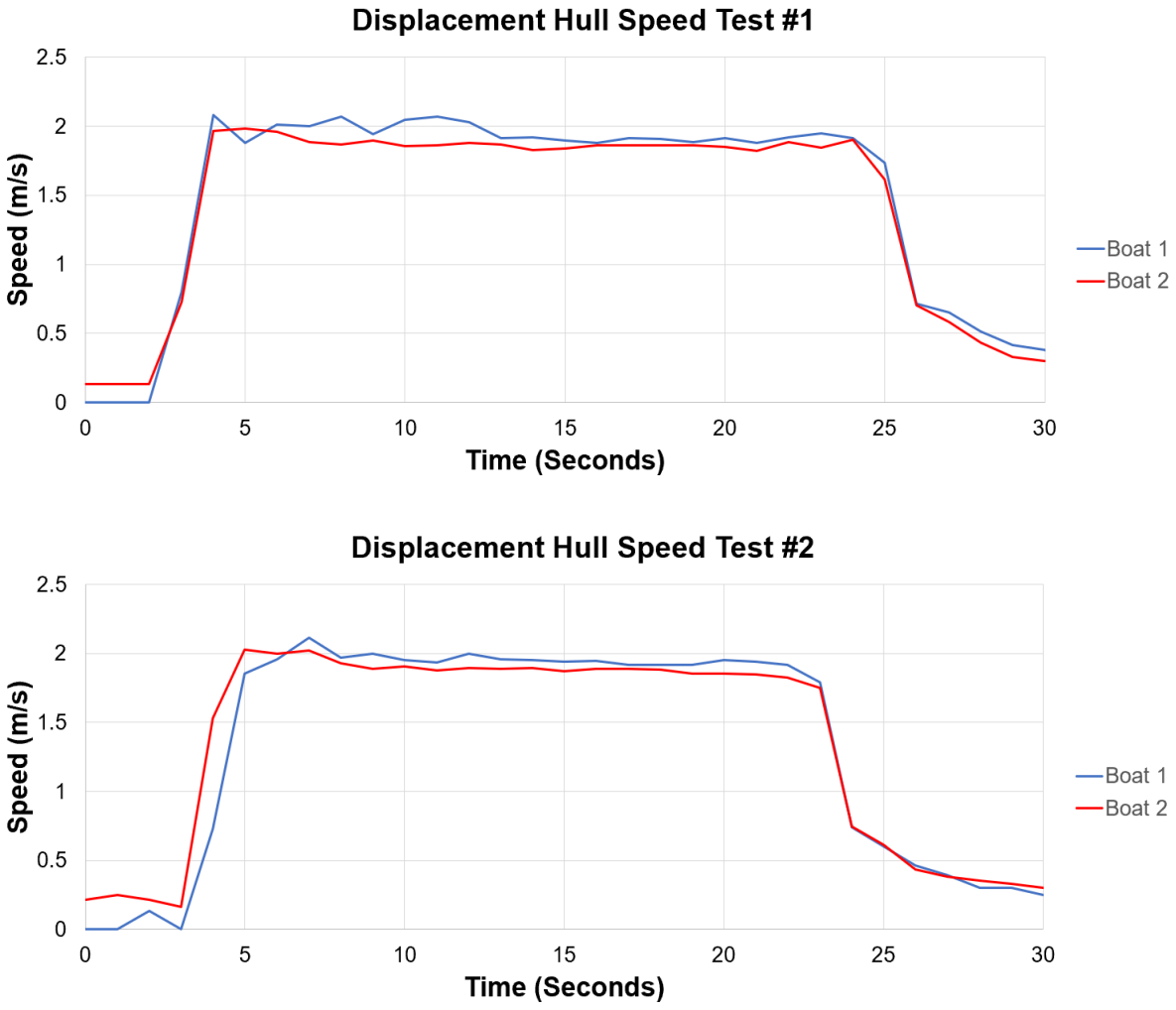

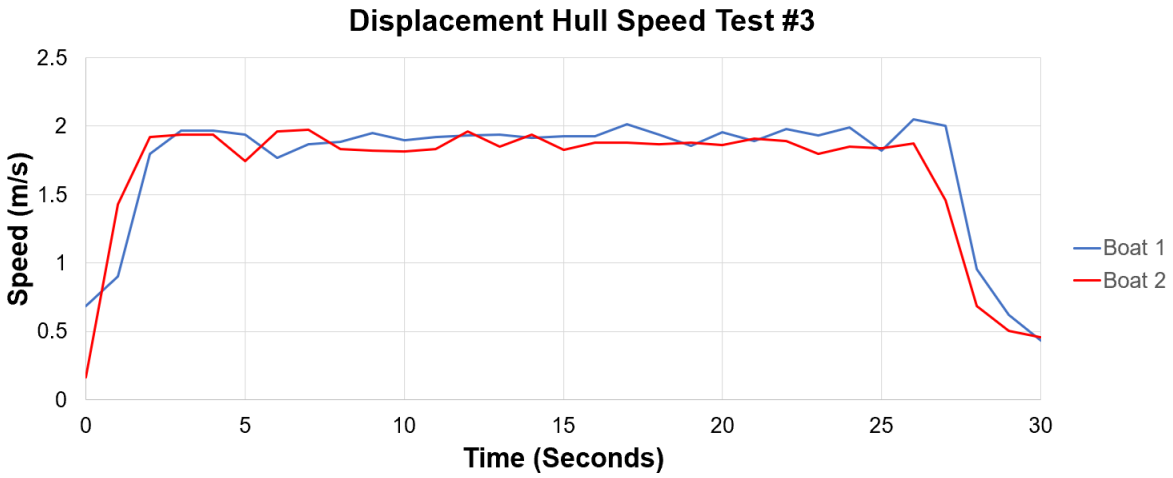
Displacement Hull Speed Test #3
Speed (m/s)
Time (Seconds)
Boat 1
Boat 2

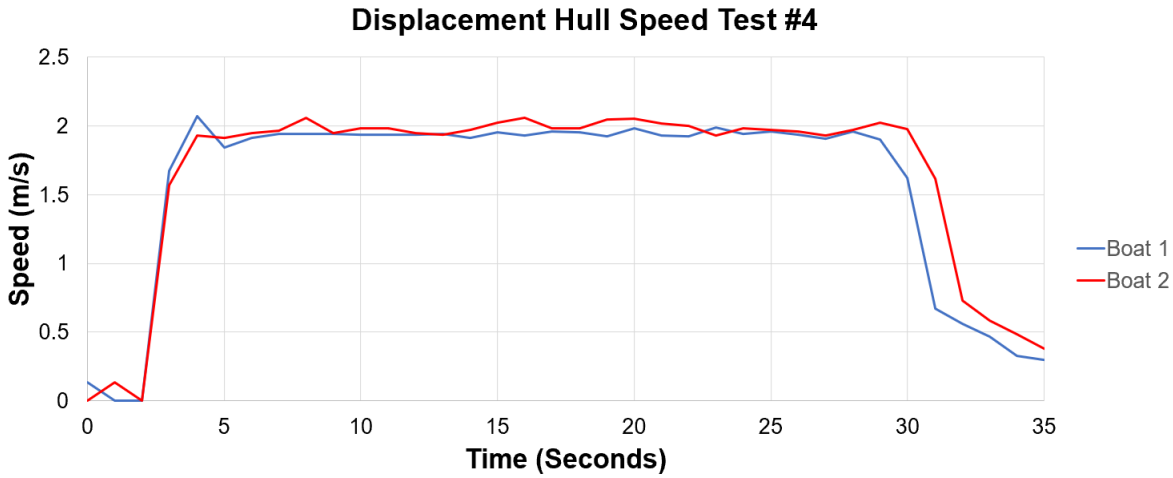
Displacement Hull Speed Test #4
Speed (m/s)
Time (Seconds)
Boat 1
Boat 2

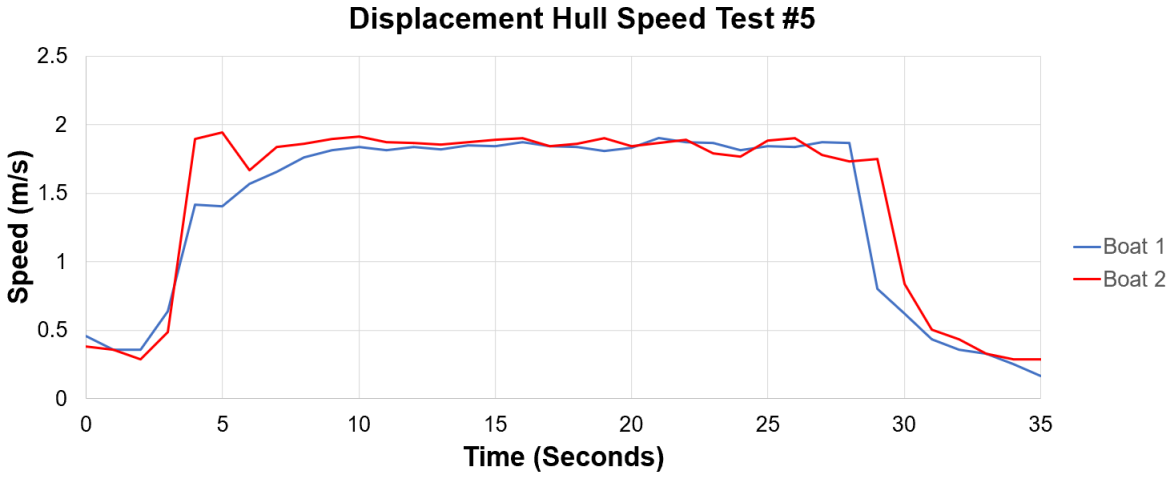
Displacement Hull Speed Test #5
Speed (m/s)
Time (Seconds)
Boat 1
Boat 2

Figure 3.15: Speed tests performed at low speed (75% throttle limit) such that the model boats behave as displacement hulls. Note that the GPS device has an error of ±0.2 m/s.

For the speed tests at 75% throttle limit, the boats were run in a straight line for roughly 20 seconds at steady state speed in five different trials. Boat 1 and Boat 2 both had an average steady speed of 1.9±0.2 m/s. By studying an image of the boats at traveling 75% throttle in ImageJ software, the wetted length of the boat is determined. As can be seen in Figure 3.16, ImageJ analysis concluded that the wetted length of the model boat at 75% throttle is approximately 19.5±0.5 inches. The margin of error is caused by the fact that the wetted length fluctuates as the boat travels over ripples on the lake water's surface.

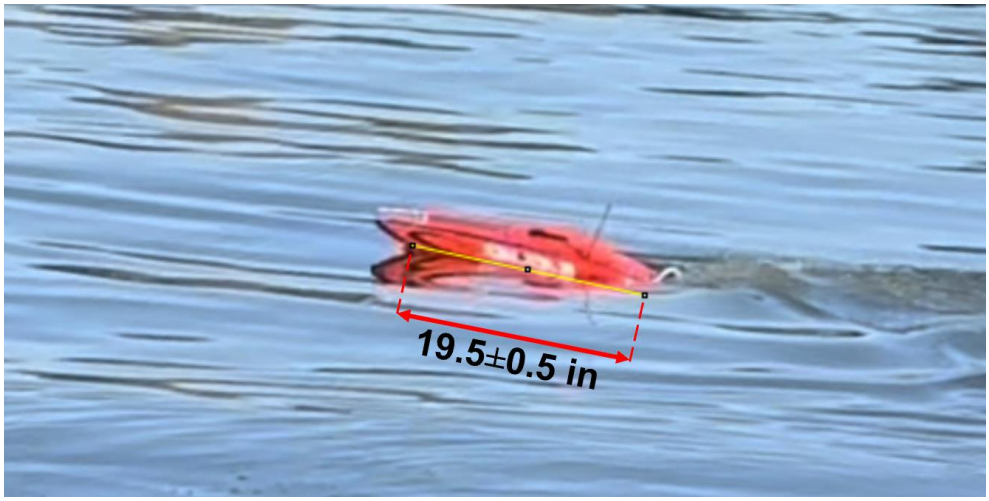

Figure 3.16: An image of the model boat traveling at 75% throttle, such that it acts as a displacement hull. This image is uploaded to ImageJ software to determine visually (i.e., via pixel count) that the wetted length is approximately 19.5±0.5 inches.

The Reynolds number Re_x of the flow is calculated using Equation 3.2, where ρ is the water's density, μ is the water's dynamic viscosity, U is hull speed, and L is the wetted length of the model boat.

$$\mathrm{Re}_x = \frac{\rho \times U \times L}{\mu} \tag{3.2}$$

It is assumed that the lake water is fresh water at 10°C, where ρ is 999.7 kg/m^3 and μ is 1.308×10^{-3} kg·m^{-1}·s^{-1}. At a hull speed of 1.9±0.2 m/s and wetted length of 19.5±0.5 inches, Equation 3.2 yields a Reynold's number of $Re_x = (7.2\pm0.9)\times10^5$. Assuming the wetted surface of the hull is modelled as a flat plate, this Reynold number means the boat is experiencing transitional flow, since $5\times10^5 < Re_x < 3\times10^6$ [153].

To make the model boats experience fully turbulent flow, the boats must be driven at 100% throttle, such that the boats move fast enough to begin planing. The results of the planing hull tests are shown in Figure 3.17.

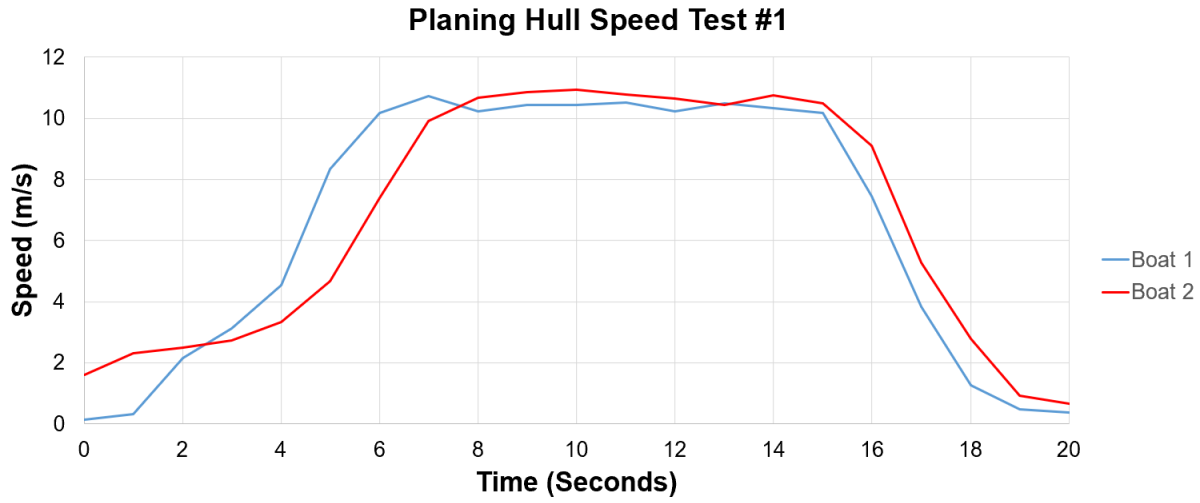
Planing Hull Speed Test #1
Speed (m/s)
Time (Seconds)
Boat 1
Boat 2

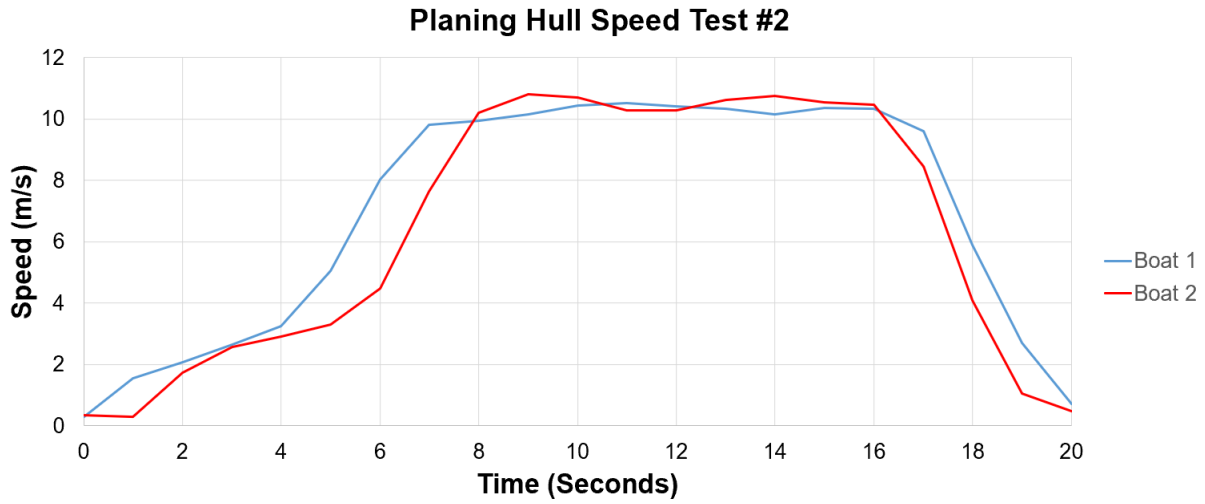
Planing Hull Speed Test #2
Speed (m/s)
Time (Seconds)
Boat 1
Boat 2

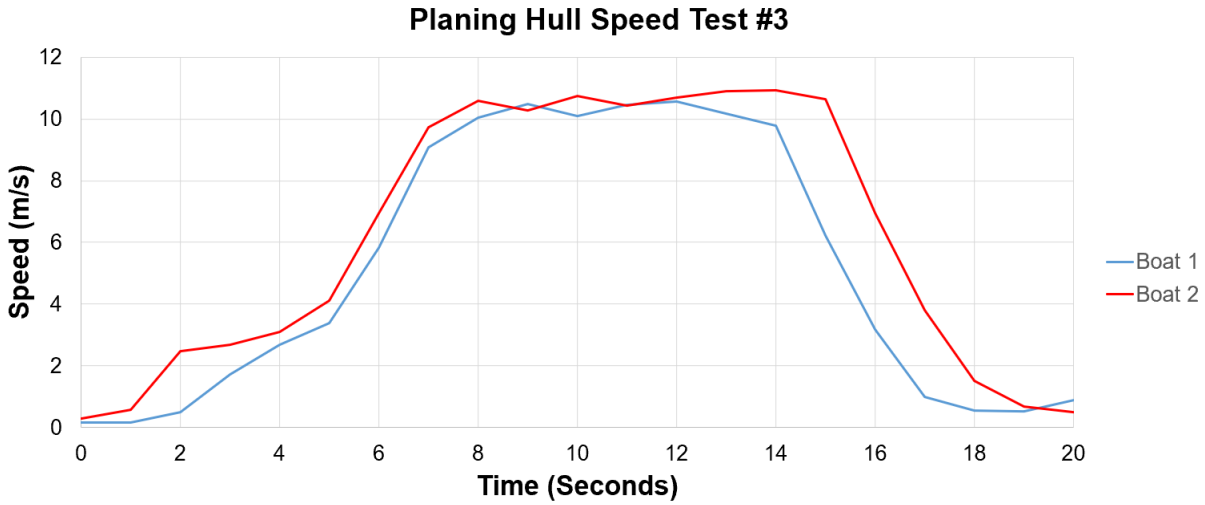
Planing Hull Speed Test #3
Speed (m/s)
Time (Seconds)
Boat 1
Boat 2

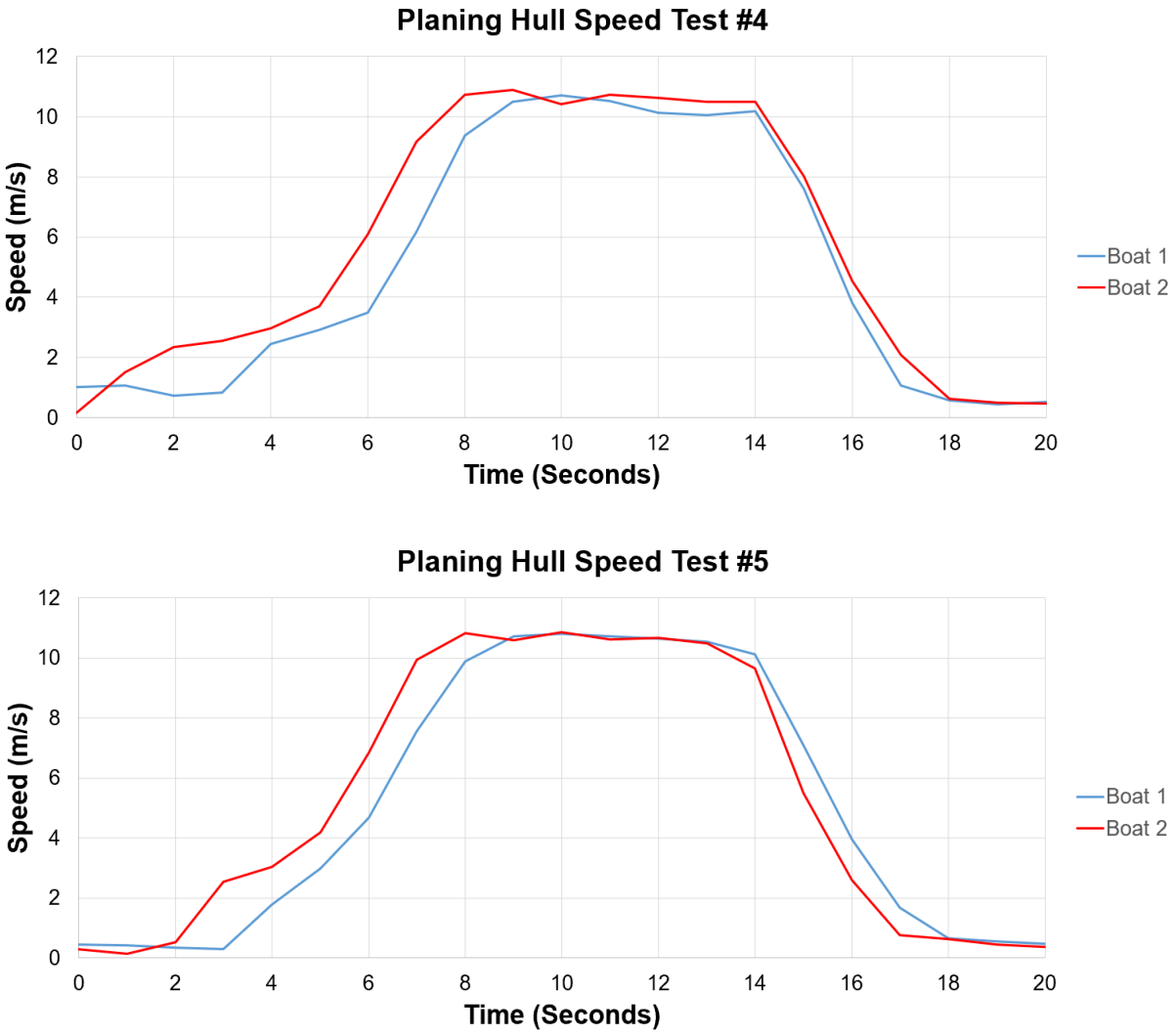

Figure 3.17: Speed tests performed at high speed (100% throttle limit) such that the model boats behave as planing hulls. Note that the GPS device has an error of ±0.2 m/s.

For 100% throttle limit tests, the boats were run in a straight line for roughly 10 seconds at steady planing speed in five different trials. The durations of tests were limited to 10 seconds of steady planing, since after that time the boats are too far away for the boat driver to see, making them difficult to steer safely. Boat 1 and Boat 2 reached steady state speeds of 10.3±0.2 m/s and

10.5±0.2 m/s, respectively, yielding a percent difference of 2%. The small difference in speeds between the boats are due to the fact that the boats are more significantly disturbed by ripples on the lake's surface when planing, making it difficult to record perfectly steady trials. As can be seen in Figure 3.18, ImageJ analysis concluded that the wetted length of the model boat when planing at 100% throttle is approximately 18.0±0.5 inches.

Figure 3.18: An image of the model boat traveling at 100% throttle, such that it acts as a planing hull. This image is uploaded to ImageJ software to determine visually (i.e., via pixel count) that the wetted length is approximately 18.0±0.5 inches.

At a hull speed of 10.3±0.2 m/s and wetted length of 18.0±0.5 inches, Equation 3.2 yields a Reynold's number of $Re_x = (3.6\pm0.2)\times10^6$. At a hull speed of 10.5±0.2 m/s, Equation 3.2 yields a Reynold's number of $Re_x = (3.7\pm0.2)\times10^6$. Assuming the wetted surface of the hull is modelled as a flat plate, this Reynold number infers that the boat is experiencing turbulent flow, since $Re_x > 3\times10^6$. Hence, it is shown that this experimental procedure can be used to test SHPo samples in

turbulent, open-water conditions to study the effect of SHPo drag reduction on the overall performance of marine vessels.

Chapter 4: Conclusion

4.1 Overview

SHPo surfaces are an important emerging technology due to their potential ability to passively produce drag reduction on marine vessels, which would reduce fuel costs and pollutant emissions. The cargo shipping industry is a promising opportunity for SHPo surfaces to find financial success as a commercial product, since these large ships each use thousands of metric tons of fuel every year to complete their busy schedules. By making predictions for the methods and costs of manufacturing and selling SHPo surfaces, it is estimated that the ROI of applying SHPo surfaces on a typical cargo ship for a 2.5-year lifespan is between 338% and 562%, depending on which material is used to fabricate the surfaces. SHPo surfaces may also provide tremendous value to speedboats, since the drag reduction produced by SHPo surfaces would increase these vessels' top speed. It is estimated that SHPo surfaces can increase the top speed of a luxury powerboat by 7%, while only costing roughly 1.5% of the total price of purchasing the boat. SHPo surfaces may also become an environmentally friendly alternative to toxic antifouling paint, although the effectiveness of SHPo surfaces' anti-fouling properties in practical conditions is yet to be proven unequivocally.

While the drag reduction of SHPo surfaces has been studied extensively in laminar flows, a better understanding of SHPo drag reduction in turbulent flows has only been achieved in the last few years. Additionally, most of the turbulent flow studies conducted so far have been in water tunnels, which often produce misleading, over-optimistic results. This paper devises a new procedure for testing SHPo surfaces in a natural body of water and turbulent flow conditions, by comparing the speed of a modified model boat with SHPo surfaces to an identical model boat

without them. When testing in turbulent flow conditions with a Reynolds number of approximately $Re_x = (3.6\pm0.2)\times10^6$, the two model boats fabricated for this testing procedure have an average steady speed of 10.3±0.2 m/s and 10.5±0.2 m/s, yielding a percent difference of only 2%. In transitional flow conditions with $Re_x = (7.2\pm0.9)\times10^5$, both of the two model boats fabricated for this testing procedure have an average steady speed of 1.9±0.2 m/s, yielding a percent difference of 0%.

4.2 Future Work

The model boat testing procedure introduced in this paper is intended to be used to test SHPo film samples that will be fabricated in the future. These samples will likely be made with PDMS, PTFE, fluoroacrylate polymer, or 80A Resin, because these materials are low-cost, flexible, and have inherent hydrophobic material properties. The effect of these substrate materials on drag reduction has not yet been studied. The samples will likely be produced using a photolithographically fabricated metal mold, which has the negative microstructure of the SHPo microstructure. This model boat testing procedure can then be used to study the drag reduction of these film samples, so that the SHPo samples made during the development of R2R process can be tested quickly for pre-screening before using a larger boat.

Appendix

The estimate bulk order pricing of polydimethylsiloxane (PDMS, CAS# 63148-62-9) was found to be $19,885.49 per 2204.6 pounds of PDMS, from the website of Applied Material Solutions [154]. PDMS has a density of 0.919 grams per cm^3, so the unit price of PDMS is $69.18 per gallon. The bulk-order pricing of 80A Resin, fluoroacrylate, and Teflon (PTFE) were acquired by reaching out to suppliers for a price estimate. The communications with these suppliers are shown in Figures A.1, A.2, and A.3. The price of 80A resin from the company Source Graphics is $199.00 per liter before shipping. For bulk orders of more than 600 liters the price is discounted by 30%. Hence, the price of 80A Resin is $139.30 per liter, or $527.31 per gallon. The price of fluoroacrylate from the company Cytonix is $78.18 per pound. Their product is called FluorAcryl 3298, which is a UV-curable fluoroacrylate oligomer with a density of approximately 1.8 pounds per liter. Hence, the price of 80A Resin is $532.71 per gallon. The price of Teflon (PTFE) powder from the company Fluorogistx is $19.78 per pound. Their Teflon 7AX product has a density of 460 grams per liter, so the unit price is $75.92 per gallon.

Formlabs Flexible 80A Resin Inbox ×

Noah Demeke <noah.d@sourcegraphics.com>
to me

Hi Christopher,

Thank you for your interest in Formlab products! My name is Noah and I am your dedicated supplies representative here at Source Graphics. It is a pleasure to work with you!

Since you are associated with a university, I am able to offer a 3.5% educational discount for all orders. I have also attached our official bulk discount offer for your reference.

If you have any questions, please do not hesitate to contact me via email at noah.d@sourcegraphics.com or my direct line 714-463-1906 and I will be more than happy to assist.

Thanks again, Christopher. We appreciate the opportunity to work with you and earn your business!

Best Regards,

SourceGraphics

Noah Demeke
Supplies Representative
Source Graphics

800-791-9042, ext. 106 | 714-463-1906
noah.d@sourcegraphics.com
sourcegraphics.com
1530 N. Harmony Circle, Anaheim, CA, 92807

One attachment • Scanned by Gmail

Bulk Purchase (L)	Bulk discounting
30	7%
60	9%
120	12%
180	15%
300	20%
420	25%
600	30%

(a)

Bulk Purchase (L)	Bulk discounting
30	7%
60	9%
120	12%
180	15%
300	20%
420	25%
600	30%

(b)

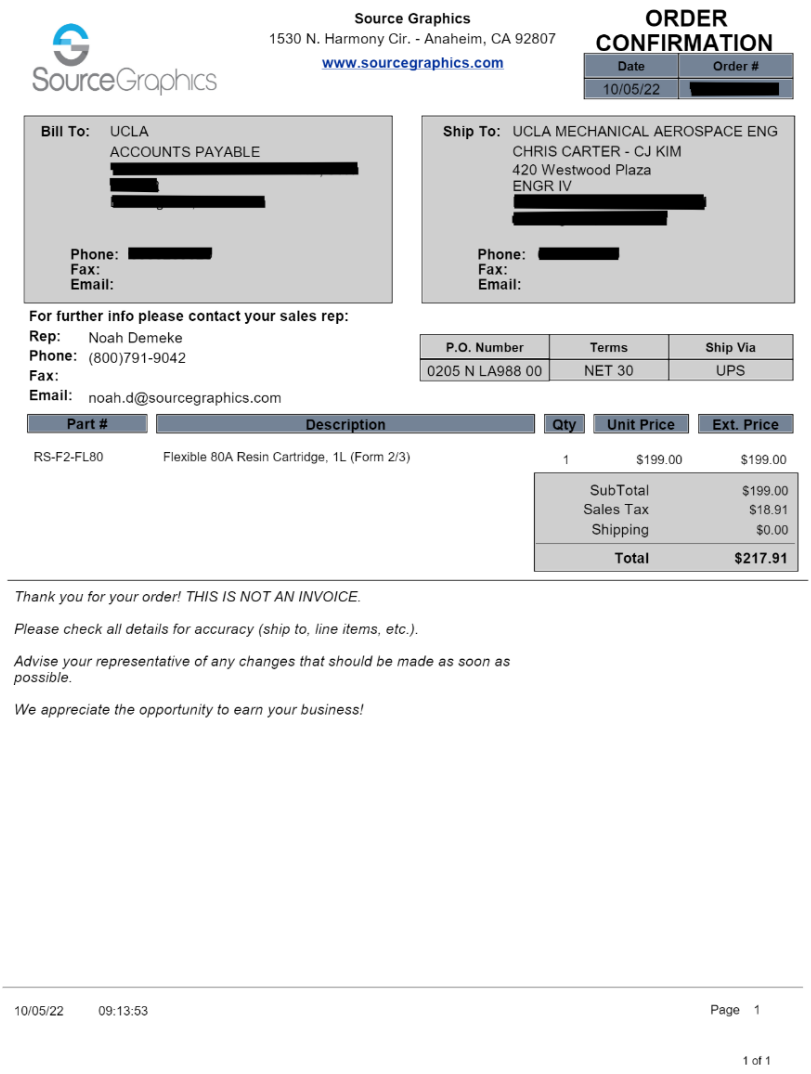

Source Graphics
1530 N. Harmony Cir. - Anaheim, CA 92807
www.sourcegraphics.com

ORDER CONFIRMATION

Date	Order #
10/05/22	[redacted]

Bill To: UCLA
ACCOUNTS PAYABLE
[redacted]
Phone: [redacted]
Fax:
Email:

Ship To: UCLA MECHANICAL AEROSPACE ENG
CHRIS CARTER - CJ KIM
420 Westwood Plaza
ENGR IV
[redacted]
Phone: [redacted]
Fax:
Email:

For further info please contact your sales rep:
Rep: Noah Demeke
Phone: (800)791-9042
Fax:
Email: noah.d@sourcegraphics.com

P.O. Number	Terms	Ship Via
0205 N LA988 00	NET 30	UPS

Part #	Description	Qty	Unit Price	Ext. Price
RS-F2-FL80	Flexible 80A Resin Cartridge, 1L (Form 2/3)	1	$199.00	$199.00

SubTotal	$199.00
Sales Tax	$18.91
Shipping	$0.00
Total	**$217.91**

Thank you for your order! THIS IS NOT AN INVOICE.

Please check all details for accuracy (ship to, line items, etc.).

Advise your representative of any changes that should be made as soon as possible.

We appreciate the opportunity to earn your business!

10/05/22 09:13:53 Page 1

1 of 1

(c)

Figure A.1: Price information for the 80A Resin. (a) Email communication with a sales representative from Source Graphics providing the bulk-order discounts. (b) The bulk order discounts that were provided. (c) Order of a small quantity of 80A Resin, showing that the standard price is $199.00 per liter.

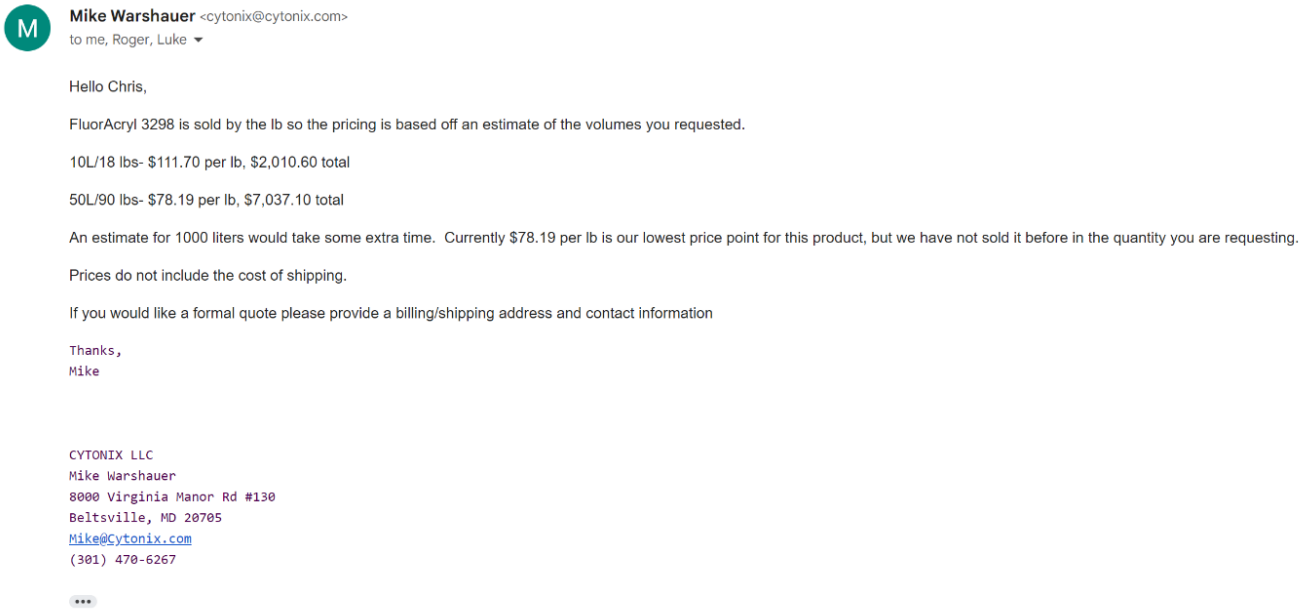

Mike Warshauer <cytonix@cytonix.com>
to me, Roger, Luke

Hello Chris,

FluorAcryl 3298 is sold by the lb so the pricing is based off an estimate of the volumes you requested.

10L/18 lbs- $111.70 per lb, $2,010.60 total

50L/90 lbs- $78.19 per lb, $7,037.10 total

An estimate for 1000 liters would take some extra time. Currently $78.19 per lb is our lowest price point for this product, but we have not sold it before in the quantity you are requesting.

Prices do not include the cost of shipping.

If you would like a formal quote please provide a billing/shipping address and contact information

Thanks,
Mike

CYTONIX LLC
Mike Warshauer
8000 Virginia Manor Rd #130
Beltsville, MD 20705
Mike@Cytonix.com
(301) 470-6267

Figure A.2: Price information for the fluoroacrylate polymer from a sales representative from Cytonix. The bulk-order price of their FluorAcryl 3298 product is $79.19 per pound.

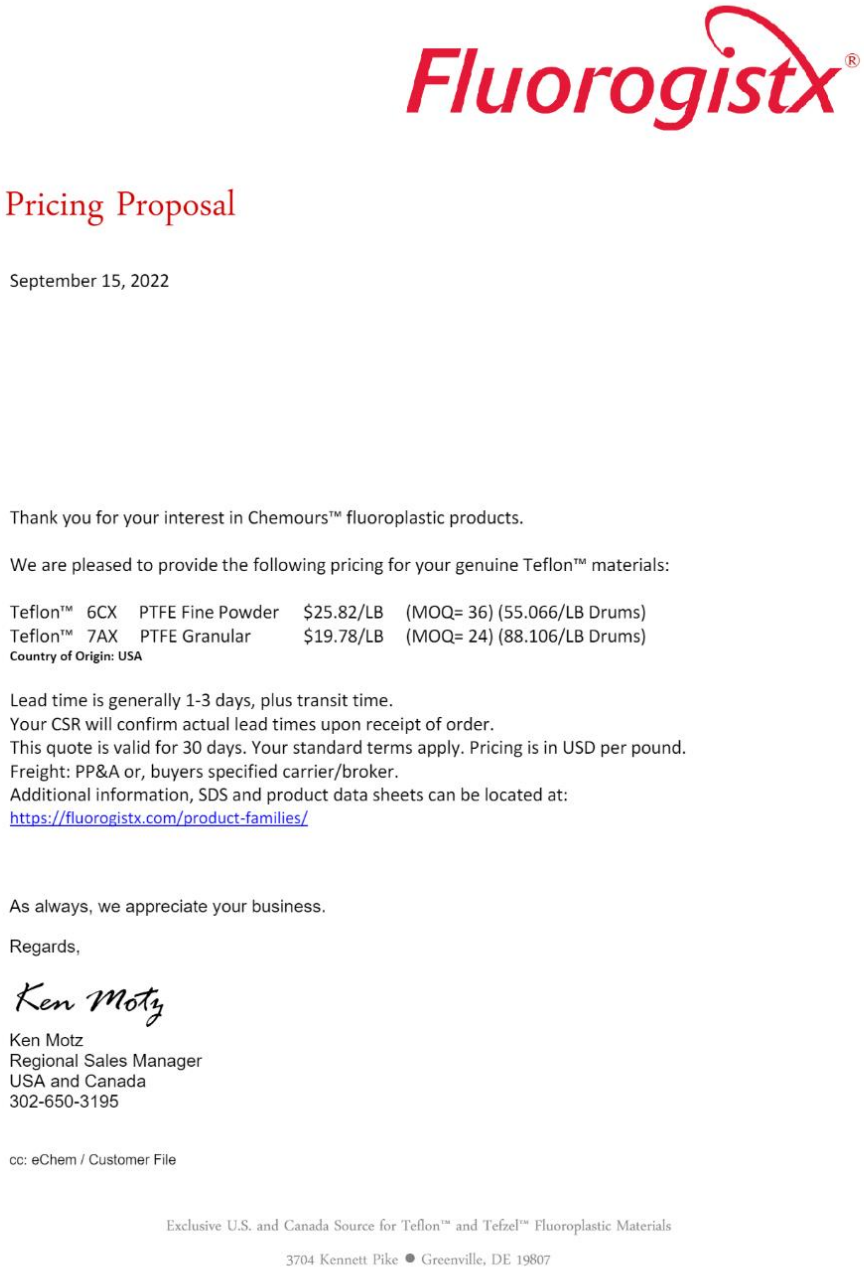

Fluorogistx®

Pricing Proposal

September 15, 2022

Thank you for your interest in Chemours™ fluoroplastic products.

We are pleased to provide the following pricing for your genuine Teflon™ materials:

Teflon™	6CX	PTFE Fine Powder	$25.82/LB	(MOQ= 36) (55.066/LB Drums)
Teflon™	7AX	PTFE Granular	$19.78/LB	(MOQ= 24) (88.106/LB Drums)

Country of Origin: USA

Lead time is generally 1-3 days, plus transit time.
Your CSR will confirm actual lead times upon receipt of order.
This quote is valid for 30 days. Your standard terms apply. Pricing is in USD per pound.
Freight: PP&A or, buyers specified carrier/broker.
Additional information, SDS and product data sheets can be located at:
https://fluorogistx.com/product-families/

As always, we appreciate your business.

Regards,

Ken Motz

Ken Motz
Regional Sales Manager
USA and Canada
302-650-3195

cc: eChem / Customer File

Exclusive U.S. and Canada Source for Teflon™ and Tefzel™ Fluoroplastic Materials

3704 Kennett Pike ● Greenville, DE 19807

Figure A.3: Price information for Teflon PTFE from a sales representative from Flurogistx. The bulk-order price of their Teflon 7AX PTFE product is $19.78 per pound.

Bibliography

[1] J. Ou, B. Perot, and J. P. Rothstein, “Laminar drag reduction in microchannels using ultrahydrophobic surfaces,” *Physics of Fluids*, vol. 16, no. 12, pp. 4635–4643, Nov. 2004.

[2] C.-H. Choi and C.-J. Kim, “Large slip of aqueous liquid flow over a nanoengineered superhydrophobic surface,” *Physical Review Letters*, vol. 96, no. 6, Feb. 2006.

[3] W. Barthlott and C. Neinhuis, “Purity of the sacred Lotus, or escape from contamination in biological surfaces,” *Planta*, vol. 202, no. 1, pp. 1–8, Apr. 1997.

[4] L. Cao, A. K. Jones, V. K. Sikka, J. Wu, and D. Gao, “Anti-icing superhydrophobic coatings,” *Langmuir*, vol. 25, no. 21, pp. 12444–12448, Oct. 2009.

[5] A. Marmur, “Super-hydrophobicity fundamentals: Implications to biofouling prevention,” *Biofouling*, vol. 22, no. 2, pp. 107–115, Jan. 2006.

[6] T. Liu, Y. Yin, S. Chen, X. Chang, and S. Cheng, “Super-hydrophobic surfaces improve corrosion resistance of copper in seawater,” *Electrochimica Acta*, vol. 52, no. 11, pp. 3709–3713, Mar. 2007.

[7] N. Yu, “Plastron State and Drag Reduction of High-Performance Superhydrophobic (SHPo) Surfaces in High-Speed Turbulent Flows on Open Water,” Ph.D. dissertation, University of California, Los Angeles., Los Angeles, CA, 2022.

[8] H. Park, C.-H. Choi, and C.-J. Kim, “Superhydrophobic drag reduction in turbulent flows: A critical review,” *Experiments in Fluids*, vol. 62, no. 11, Oct. 2021.

[9] J. Hua, C.-W. Cheng, and D.-S. Hwang, “Total life cycle emissions of post-Panamax containerships powered by conventional fuel or natural gas,” *Journal of the Air & Waste Management Association*, vol. 69, no. 2, pp. 131–144, Dec. 2018.

[10] K. Fukuda, J. Tokunaga, T. Nobunaga, T. Nakatani, T. Iwasaki, and Y. Kunitake, "Frictional drag reduction with air lubricant over a super-water-repellent surface," *Journal of Marine Science and Technology*, vol. 5, no. 3, pp. 123–130, Dec. 2000.

[11] C. Lee, C.-H. Choi, and C.-J. Kim, "Superhydrophobic drag reduction in Laminar Flows: A critical review," *Experiments in Fluids*, vol. 57, no. 12, Nov. 2016.

[12] R. N. Wenzel, "Resistance of solid surfaces to wetting by water," *Industrial & Engineering Chemistry*, vol. 28, no. 8, pp. 988–994, Mar. 1936.

[13] C.-J. Kim, "Smooth sailing," *Physics World*, 18-May-2017. [Online]. Available: https://physicsworld.com/a/smooth-sailing/. [Accessed: 13-Nov-2022].

[14] J. Kim and C.-J. Kim, "Nanostructured surfaces for dramatic reduction of flow resistance in droplet-based microfluidics," *Technical Digest. MEMS 2002 IEEE International Conference. Fifteenth IEEE International Conference on Micro Electro Mechanical Systems (Cat. No.02CH37266)*, pp. 479–482, Aug. 2002.

[15] T. L. Liu, Z. Chen, and C.-J. Kim, "A dynamic Cassie–Baxter model," *Soft Matter*, vol. 11, no. 8, pp. 1589–1596, Jan. 2015.

[16] A. B. Cassie and S. Baxter, "Wettability of porous surfaces," *Transactions of the Faraday Society*, vol. 40, pp. 546–551, Jun. 1944.

[17] J. P. Rothstein, "Slip on superhydrophobic surfaces," *Annual Review of Fluid Mechanics*, vol. 42, no. 1, pp. 89–109, Jan. 2010.

[18] K. Watanabe, Y. Udagawa, and H. Udagawa, "Drag reduction of newtonian fluid in a circular pipe with a highly water-repellent wall," *Journal of Fluid Mechanics*, vol. 381, pp. 225–238, Feb. 1999.

[19] C.-H. Choi, J. Kim, and C.-J. Kim, “Nanoturf surfaces for reduction of liquid flow drag in Microchannels,” *NSF Nanoscale Science and Engineering Grantees Conference*, Dec. 2002.

[20] C.-H. Choi, U. Ulmanella, J. Kim, C.-M. Ho, and C.-J. Kim, “Effective slip and friction reduction in nanograted superhydrophobic microchannels,” *Physics of Fluids*, vol. 18, no. 087105, pp. 1–8, Aug. 2006.

[21] M. Xu, G. Sun, and C.-J. Kim, “Infinite lifetime of underwater superhydrophobic states,” *Physical Review Letters*, vol. 113, no. 13, pp. 1–5, Sep. 2014.

[22] J. Ou and J. P. Rothstein, “Direct velocity measurements of the flow past drag-reducing ultrahydrophobic surfaces,” *Physics of Fluids*, vol. 17, no. 10, pp. 1–12, Oct. 2005.

[23] J. Davies, D. Maynes, B. W. Webb, and B. Woolford, “Laminar flow in a microchannel with superhydrophobic walls exhibiting transverse ribs,” *Physics of Fluids*, vol. 18, no. 8, pp. 1–11, Aug. 2006.

[24] R. Truesdell, A. Mammoli, P. Vorobieff, F. van Swol, and C. J. Brinker, “Drag reduction on a patterned superhydrophobic surface,” *Physical Review Letters*, vol. 97, no. 4, pp. 1–4, Jul. 2006.

[25] D. Maynes, K. Jeffs, B. Woolford, and B. W. Webb, “Laminar flow in a microchannel with hydrophobic surface patterned microribs oriented parallel to the flow direction,” *Physics of Fluids*, vol. 19, no. 9, pp. 1–12, Sep. 2007.

[26] A. Steinberger, C. Cottin-Bizonne, P. Kleimann, and E. Charlaix, “High friction on a bubble mattress,” *Nature Materials*, vol. 6, no. 9, pp. 665–668, Jul. 2007.

[27] D. Byun, J. Kim, H. S. Ko, and H. C. Park, “Direct measurement of slip flows in superhydrophobic microchannels with transverse grooves,” *Physics of Fluids*, vol. 20, no. 11, pp. 1–9, Nov. 2008.

[28] C. Lee, C.-H. Choi, and C.-J. Kim, “Structured surfaces for a giant liquid slip,” *Physical Review Letters*, vol. 101, no. 6, pp. 1–4, Aug. 2008.

[29] P. Tsai, A. M. Peters, C. Pirat, M. Wessling, R. G. Lammertink, and D. Lohse, “Quantifying effective slip length over micropatterned hydrophobic surfaces,” *Physics of Fluids*, vol. 21, no. 11, pp. 1–8, Nov. 2009.

[30] Y. C. Jung and B. Bhushan, “Biomimetic structures for fluid drag reduction in laminar and turbulent flows,” *Journal of Physics: Condensed Matter*, vol. 22, no. 3, pp. 1–9, Dec. 2009.

[31] C. Lee and C.-J. Kim, “Influence of surface hierarchy of superhydrophobic surfaces on Liquid Slip,” *Langmuir*, vol. 27, no. 7, pp. 4243–4248, Mar. 2011.

[32] N. Kashaninejad, N.-T. Nguyen, and W. K. Chan, “Eccentricity effects of microhole arrays on drag reduction efficiency of microchannels with a hydrophobic wall,” *Physics of Fluids*, vol. 24, no. 11, pp. 1–18, Nov. 2012.

[33] T. J. Kim and C. Hidrovo, “Pressure and partial wetting effects on superhydrophobic friction reduction in microchannel flow,” *Physics of Fluids*, vol. 24, no. 11, pp. 1–18, Nov. 2012.

[34] A. Maali, Y. Pan, B. Bhushan, and E. Charlaix, “Hydrodynamic drag-force measurement and slip length on microstructured surfaces,” *Physical Review E*, vol. 85, no. 6, pp. 1–5, Jun. 2012.

[35] E. Karatay, A. S. Haase, C. W. Visser, C. Sun, D. Lohse, P. A. Tsai, and R. G. Lammertink, "Control of slippage with tunable bubble mattresses," *Proceedings of the National Academy of Sciences*, vol. 110, no. 21, pp. 8422–8426, Mar. 2013.

[36] G. Bolognesi, C. Cottin-Bizonne, and C. Pirat, "Evidence of slippage breakdown for a superhydrophobic microchannel," *Physics of Fluids*, vol. 26, no. 8, pp. 1–11, Aug. 2014.

[37] A. Lee and H.-Y. Kim, "Does liquid slippage within a rough channel always increase the flow rate?," *Physics of Fluids*, vol. 26, no. 7, pp. 1–10, Jul. 2014.

[38] K. Watanabe, T. Takayama, S. Ogata, and S. Isozaki, "Flow between two coaxial rotating cylinders with a highly water-repellent wall," *AIChE Journal*, vol. 49, no. 8, pp. 1956–1963, Apr. 2003.

[39] S. Gogte, P. Vorobieff, R. Truesdell, A. Mammoli, F. van Swol, P. Shah, and C. J. Brinker, "Effective slip on textured superhydrophobic surfaces," *Physics of Fluids*, vol. 17, no. 5, pp. 1–4, Apr. 2005.

[40] P. Joseph, C. Cottin-Bizonne, J.-M. Benoît, C. Ybert, C. Journet, P. Tabeling, and L. Bocquet, "Slippage of water past superhydrophobic carbon nanotube forests in Microchannels," *Physical Review Letters*, vol. 97, no. 15, pp. 1–4, Oct. 2006.

[41] B. Bhushan, Y. Wang, and A. Maali, "Boundary Slip study on hydrophilic, hydrophobic, and superhydrophobic surfaces with dynamic atomic force microscopy," *Langmuir*, vol. 25, no. 14, pp. 8117–8121, Apr. 2009.

[42] R. N. Govardhan, G. S. Srinivas, A. Asthana, and M. S. Bobji, "Time dependence of effective slip on textured hydrophobic surfaces," *Physics of Fluids*, vol. 21, no. 5, pp. 1–8, May 2009.

[43] N. J. Shirtcliffe, G. McHale, M. I. Newton, and Y. Zhang, “Superhydrophobic copper tubes with possible flow enhancement and drag reduction,” *ACS Applied Materials & Interfaces*, vol. 1, no. 6, pp. 1316–1323, Jun. 2009.

[44] Y. Wang, B. Bhushan, and A. Maali, “Atomic force microscopy measurement of boundary slip on hydrophilic, hydrophobic, and superhydrophobic surfaces,” *Journal of Vacuum Science & Technology A: Vacuum, Surfaces, and Films*, vol. 27, no. 4, pp. 754–760, Jun. 2009.

[45] D. Kim and W. Hwang, “A template-based superhydrophobic tube structure with nanofiber forests and its mass flow characteristic,” *Journal of Micromechanics and Microengineering*, vol. 20, no. 2, pp. 1–5, Jan. 2010.

[46] J. Li, M. Zhou, X. Ye, and L. Cai, “Self-comparison measurement for slippage on superhydrophobic surfaces based on the wetting transition,” *Journal of Micromechanics and Microengineering*, vol. 20, no. 11, pp. 1–5, Oct. 2010.

[47] Y. Wang and B. Bhushan, “Boundary Slip and nanobubble study in micro/nanofluidics using atomic force microscopy,” *Soft Matter*, vol. 6, no. 1, pp. 29–66, Jan. 2010.

[48] Z. Ming, L. Jian, W. Chunxia, Z. Xiaokang, and C. Lan, “Fluid drag reduction on superhydrophobic surfaces coated with carbon nanotube forests (CNTS),” *Soft Matter*, vol. 7, no. 9, pp. 4391–4396, Apr. 2011.

[49] D. J. Lee, K. Y. Cho, S. Jang, Y. S. Song, and J. R. Youn, “Liquid slip on a nanostructured surface,” *Langmuir*, vol. 28, no. 28, pp. 10488–10494, Jun. 2012.

[50] S. Srinivasan, W. Choi, K.-C. Park, S. S. Chhatre, R. E. Cohen, and G. H. McKinley, “Drag reduction for viscous laminar flow on spray-coated non-wetting surfaces,” *Soft Matter*, vol. 9, no. 24, pp. 5691–5702, Jun. 2013.

[51] I. A. Yeginbayeva and M. Atlar, “An experimental investigation into the surface and hydrodynamic characteristics of marine coatings with mimicked Hull Roughness Ranges,” *Biofouling: The Journal of Bioadhesion and Biofilm Research*, vol. 34, no. 9, pp. 1001–1019, Dec. 2018.

[52] M. Xu, A. Grabowski, N. Yu, G. Kerezyte, J.-W. Lee, B. R. Pfeifer, and C.-J. Kim, “Superhydrophobic drag reduction for turbulent flows in Open water,” *Physical Review Applied*, vol. 13, no. 3, pp. 1–10, Mar. 2020.

[53] H. Park, G. Sun, and C.-J. Kim, “Superhydrophobic turbulent drag reduction as a function of surface grating parameters,” *Journal of Fluid Mechanics*, vol. 747, pp. 722–734, Apr. 2014.

[54] T. Min and J. Kim, “Effects of hydrophobic surface on skin-friction drag,” *Physics of Fluids*, vol. 16, no. 7, pp. 55–58, May 2004.

[55] J. Lee, T. O. Jelly, and T. A. Zaki, “Effect of Reynolds number on turbulent drag reduction by superhydrophobic surface textures,” *Flow, Turbulence and Combustion*, vol. 95, no. 2-3, pp. 277–300, Jul. 2015.

[56] A. Rastegari and R. Akhavan, “The common mechanism of turbulent skin-friction drag reduction with superhydrophobic longitudinal microgrooves and Riblets,” *Journal of Fluid Mechanics*, vol. 838, pp. 68–104, Jan. 2018.

[57] I. Arenas, E. García, M. K. Fu, P. Orlandi, M. Hultmark, and S. Leonardi, “Comparison between super-hydrophobic, liquid infused and rough surfaces: A direct numerical simulation study,” *Journal of Fluid Mechanics*, vol. 869, pp. 500–525, Apr. 2019.

[58] J. S. Wexler, I. Jacobi, and H. A. Stone, “Shear-driven failure of liquid-infused surfaces,” *Physical Review Letters*, vol. 114, no. 16, pp. 1–5, Apr. 2015.

[59] L. Piao and H. Park, “Two-dimensional analysis of air–water interface on superhydrophobic grooves under fluctuating water pressure,” *Langmuir*, vol. 31, no. 29, pp. 8022–8032, Jul. 2015.

[60] J. Seo, R. García-Mayoral, and A. Mani, “Pressure fluctuations and interfacial robustness in turbulent flows over superhydrophobic surfaces,” *Journal of Fluid Mechanics*, vol. 783, pp. 448–473, Oct. 2015.

[61] E. Aljallis, M. A. Sarshar, R. Datla, V. Sikka, A. Jones, and C.-H. Choi, “Experimental study of skin friction drag reduction on superhydrophobic flat plates in high Reynolds number boundary layer flow,” *Physics of Fluids*, vol. 25, no. 2, pp. 1–14, Feb. 2013.

[62] H. Dong, M. Cheng, Y. Zhang, H. Wei, and F. Shi, “Extraordinary drag-reducing effect of a superhydrophobic coating on a macroscopic model ship at High Speed,” *Journal of Materials Chemistry A*, vol. 1, no. 19, pp. 5886–5891, Mar. 2013.

[63] C. G. Jiang, S. C. Xin, and C. W. Wu, “Drag reduction of a miniature boat with superhydrophobic grille bottom,” *AIP Advances*, vol. 1, no. 3, pp. 1–8, Aug. 2011.

[64] S. Zhang, X. Ouyang, J. Li, S. Gao, S. Han, L. Liu, and H. Wei, “Underwater drag-reducing effect of superhydrophobic submarine model,” *Langmuir*, vol. 31, no. 1, pp. 587–593, Dec. 2014.

[65] C.-H. Xue, S.-T. Jia, J. Zhang, and J.-Z. Ma, “Large-area fabrication of superhydrophobic surfaces for practical applications: An overview,” *Science and Technology of Advanced Materials*, vol. 11, no. 3, pp. 1–15, Jul. 2010.

[66] M. D. Islam, H. Perera, B. Black, M. Phillips, M. J. Chen, G. Hodges, A. Jackman, Y. Liu, C. J. Kim, M. Zikry, S. Khan, Y. Zhu, M. Pankow, and J. E. Ryu, “Template-free scalable fabrication of linearly periodic microstructures by controlling ribbing defects

phenomenon in forward roll coating for multifunctional applications," *Advanced Materials Interfaces*, vol. 9, no. 27, pp. 1–16, Aug. 2022.

[67] C. N. Niu, J. Y. Han, S. P. Hu, D. Y. Chao, X. G. Song, M. M. R. Howlader, and J. Cao, "Fast and environmentally friendly fabrication of superhydrophilic-superhydrophobic patterned aluminum surfaces," *Surfaces and Interfaces*, vol. 22, p. 100830, Nov. 2020.

[68] S. H. Ahn and L. J. Guo, "Large-area roll-to-roll and roll-to-plate nanoimprint lithography: A step toward high-throughput application of continuous nanoimprinting," *ACS Nano*, vol. 3, no. 8, pp. 2304–2310, Jul. 2009.

[69] S. Dong, Z. Wang, Y. Wang, X. Bai, Y. Q. Fu, B. Guo, C. Tan, J. Zhang, and P. A. Hu, "Roll-to-roll manufacturing of robust superhydrophobic coating on metallic engineering materials," *ACS Applied Materials & Interfaces*, vol. 10, no. 2, pp. 2174–2184, Jan. 2018.

[70] J. Li, W. Yu, D. Zheng, X. Zhao, C.-H. Choi, and G. Sun, "Hot embossing for whole Teflon superhydrophobic surfaces," *Coatings*, vol. 8, no. 7, p. 227, Jun. 2018.

[71] Y. Wang, C. Gao, W. Zhao, G. Zheng, Y. Ji, K. Dai, L. Mi, D. Zhang, C. Liu, and C. Shen, "Large-area fabrication and applications of patterned surface with anisotropic superhydrophobicity," *Applied Surface Science*, vol. 529, p. 147027, Nov. 2020.

[72] M. Xu, C. T. Liu, and C.-J. Kim, "Self-powered plastron preservation and one-step molding of semiactive superhydrophobic surfaces," *Langmuir*, vol. 36, no. 28, pp. 8193–8198, Jun. 2020.

[73] "Q1 2022 Interim Results," *A.P. Moller - Mærsk*, 04-Mar-2022. [Online]. Available: https://investor.maersk.com/static-files/b32c958d-36b6-4999-b19f-7d724cf307b6. [Accessed: 14-Nov-2022].

[74] “Q2 2021 Interim Report,” *A.P. Moller - Mærsk*, 06-Aug-2021. [Online]. Available: https://investor.maersk.com/static-files/d6de9422-29d7-497f-be1f-6970076b8ff1. [Accessed: 14-Nov-2022].

[75] K. Fukuda, J. Tokunaga, T. Nobunaga, T. Nakatani, T. Iwasaki, and Y. Kunitake, “Frictional drag reduction with air lubricant over a super-water-repellent surface,” *Journal of Marine Science and Technology*, vol. 5, no. 3, pp. 123–130, Dec. 2000.

[76] “Global average bunker price bunker prices,” *Ship & Bunker*. [Online]. Available: https://shipandbunker.com/prices/av/global/av-glb-global-average-bunker-price. [Accessed: 13-Nov-2022].

[77] “Average bunker prices,” *Ship & Bunker*. [Online]. Available: https://shipandbunker.com/prices/av. [Accessed: 13-Nov-2022].

[78] G. Miller, “Yet another worry: Price of ship fuel is now highest since 2014,” *FreightWaves*, 07-Feb-2022. [Online]. Available: https://www.freightwaves.com/news/yet-another-worry-price-of-ship-fuel-is-now-highest-since-2014. [Accessed: 13-Nov-2022].

[79] U. Einemo, “VLSFO: Fact versus fiction,” *Ship & Bunker*, 28-Mar-2021. [Online]. Available: https://shipandbunker.com/news/world/566831-vlsfo-fact-versus-fiction. [Accessed: 13-Nov-2022].

[80] M. Placek, “Amount of fuel consumed by ships worldwide by Fuel Type 2020,” *Statista*, 30-Sep-2021. [Online]. Available: https://www.statista.com/statistics/1266963/amount-of-fuel-consumed-by-ships-worldwide-by-fuel-type/#main-content. [Accessed: 13-Nov-2022].

[81] “The most common types of large cargo ships, explained,” *Yieldstreet,* 29-Oct-2019. [Online]. Available: https://www.yieldstreet.com/resources/article/types-of-cargo-ships/. [Accessed: 13-Nov-2022].

[82] “Dry Bulk Vessel Fleet,” *Costamare Inc.*, 02-Nov-2022. [Online]. Available: https://www.costamare.com/dry_fleet_employment. [Accessed: 13-Nov-2022].

[83] H. Utby, “Hydrodynamic optimization of bulk and tank ship hulls,” MSc thesis, Norweigan University of Science and Technology, Trondheim, NO, 2016. [Online]. Available: https://ntnuopen.ntnu.no/ntnu-xmlui/bitstream/handle/11250/2410757/15065_FULLTEXT.pdf?sequence=1&isAllowed=y. [Accessed: 13-Nov-2022].

[84] S. Haider, Ed., “Various bulk carrier sizes and Employment Guide,” *Bulk Carrier Guide,* 2010. [Online]. Available: https://bulkcarrierguide.com/size-range.html. [Accessed: 13-Nov-2022].

[85] C. Pålsson, “The Source for Maritime Information and Insight,” *IHS Fairplay,* 2011. [Online]. Available: http://www.imsf.info/media/1167/14-chris-palsson-ihs-fairplay-ship-types-sizes.pdf. [Accessed: 13-Nov-2022].

[86] R. Ivče, M. Bakota, S. Kos, and D. Brčić, “Advanced numerical method for determining the wetted area of container ships for increased estimation accuracy of copper biocide emissions,” *Journal of Marine Science and Engineering*, vol. 8, no. 11, p. 848, Oct. 2020.

[87] H. El-Azim, “Copper emission loading from antifouling paints and their relation to industrials and waste water effluents to the Suez bay transit area,” *Egyptian Journal of Aquatic Research*, vol. 36, no. 2, Oct. 2010.

[88] A. W. Miller, I. C. Davidson, M. S. Minton, B. Steves, C. S. Moser, L. A. Drake, and G. M. Ruiz, “Evaluation of wetted surface area of commercial ships as biofouling habitat flux to the United States,” *Biological Invasions*, vol. 20, no. 8, pp. 1977–1990, Feb. 2018.

[89] J. D. Van Maanen and P. Van Oossanen, “Resistance,” *Principles of Naval Architecture*, vol. 2, pp. 1–93, Nov. 1988.

[90] M. Xu, N. Yu, J. Kim, and C.-J. “C. J. Kim, “Superhydrophobic drag reduction in high-speed towing tank,” *Journal of Fluid Mechanics*, vol. 908, no. 10, p. A6, Feb. 2021.

[91] M. Ulsh, “Roll-to-roll manufacturing Multilab collaboration,” *National Renewable Energy Laboratory*. [Online]. Available: https://www.nrel.gov/manufacturing/roll-to-roll-multilab.html. [Accessed: 13-Nov-2022].

[92] R. R. Søndergaard, M. Hösel, and F. C. Krebs, “Roll-to-roll fabrication of large area functional organic materials,” *Journal of Polymer Science Part B: Polymer Physics*, vol. 51, no. 1, pp. 16–34, 2012.

[93] “Satin black Avery Dennison™ wrap: SW900 supreme wrapping film,” *Rvinyl*. [Online]. Available: https://www.rvinyl.com/Avery-SW900-Supreme-Wrapping-Film-Satin-Satin-Black-Vinyl. [Accessed: 13-Nov-2022].

[94] “3M FastBond Contact Cement, 5 gal, Pail,” *Zoro*. [Online]. Available: https://www.zoro.com/3m-contact-cement-5-gal-pail-85780/i/G7190635/#specifications. [Accessed: 13-Nov-2022].

[95] S. Smith, “How much glue do you need?,” *Smith & Company*, 2014. [Online]. Available: https://www.smithandcompany.org/HowMuchGlue.html. [Accessed: 13-Nov-2022].

[96] A. Sareen, R. Deters, S. Henry, and M. Selig, “Drag reduction using Riblet film applied to airfoils for wind turbines,” *49th AIAA Aerospace Sciences Meeting including the New Horizons Forum and Aerospace Exposition*, pp. 1–19, Jan. 2011.

[97] V. Stenzel, Y. Wilke, and W. Hage, “Drag-reducing paints for the reduction of fuel consumption in aviation and shipping,” *Progress in Organic Coatings*, vol. 70, no. 4, pp. 224–229, Dec. 2010.

[98] H. Kordy, “Process abilities of the Riblet-coating process with dual-cure lacquers,” *CIRP Journal of Manufacturing Science and Technology*, vol. 11, pp. 1–9, Sep. 2015.

[99] H. O. Benschop, A. J. Guerin, A. Brinkmann, M. L. Dale, A. A. Finnie, W.-P. Breugem, A. S. Clare, D. Stübing, C. Price, and K. J. Reynolds, “Drag-reducing riblets with fouling-release properties: Development and testing,” *Biofouling*, vol. 34, no. 5, pp. 532–544, May 2018.

[100] “ATMALINE RR5060/S Roll-to-Roll Screen Printing Line, R2R Screen Printer,” *ATMA Champ Ent. Corp.*, 2022. [Online]. Available: https://www.atma.com.tw/en/product/ATMALINE_RR5060-S.html. [Accessed: 13-Nov-2022].

[101] “Electricity Rates by State,” *Electric Choice*, 2022. [Online]. Available: https://www.electricchoice.com/electricity-prices-by-state/. [Accessed: 13-Nov-2022].

[102] “Economics of ship repair estimation,” *Mermaid Consultants*. [Online]. Available: https://www.mermaid-consultants.com/economics-of-ship-repair-estimation.html. [Accessed: 13-Nov-2022].

[103] “Hidramar Group Takes on Hull Repair of a Crude Oil Tanker Vessel,” *Hidramar Group*, 10-Mar-2021. [Online]. Available: https://hidramargroup.com/hidramar-group-takes-on-hull-repair-of-a-crude-oil-tanker-vessel/. [Accessed: 13-Nov-2022].

[104] D. Grossman, “Go ahead and watch this colossal cargo ship get painted,” *Popular Mechanics*, 15-Feb-2018. [Online]. Available: https://www.popularmechanics.com/technology/infrastructure/a26332/giant-ship-painted/. [Accessed: 13-Nov-2022].

[105] “Average marine painter hourly pay,” *PayScale*. [Online]. Available: https://www.payscale.com/research/US/Job=Marine_Painter/Hourly_Rate. [Accessed: 13-Nov-2022].

[106] “Hourly wage for Vehicle Wrap Installer,” *Salary.com*, 27-Oct-2022. [Online]. Available: https://www.salary.com/research/salary/posting/vehicle-wrap-installer-hourly-wages. [Accessed: 13-Nov-2022].

[107] “Price Schedule,” *Nothlake Shipyard*, 2022. [Online]. Available: https://northlakeshipyard.com/rates/. [Accessed: 13-Nov-2022].

[108] “Dry dock rates and charges,” *Fraserburgh Harbour*. [Online]. Available: http://www.fraserburgh-harbour.co.uk/dry-dock-2. [Accessed: 13-Nov-2022].

[109] “Report on Survey of U.S. Shipbuilding and Repair Facilities,” *U.S. Department of Transportation Maritime Administration*, 2001. [Online]. Available: https://www.maritime.dot.gov/sites/marad.dot.gov/files/docs/ports/national-maritime-resource-and-education-center/9476/2001-reportonsurveyofusshipbuildingandrepairfacilities.pdf. [Accessed: 13-Nov-2022].

[110] “Difference between Gross and Net Margin,” *BYJUS*, 09-Feb-2022. [Online]. Available: https://byjus.com/commerce/difference-between-gross-margin-and-net-margin/. [Accessed: 14-Nov-2022].

[111] A. Damodaran, “Margins by sector (US),” *Damodaran Online,* Jan-2022. [Online]. Available: https://pages.stern.nyu.edu/~adamodar/New_Home_Page/datafile/margin.html. [Accessed: 14-Nov-2022].

[112] P. M. Rohit, “Being square with Uncle Sam: Taxes, fees, and your boat,” *The Log*, 11-Aug-2016. [Online]. Available: https://www.thelog.com/local/being-square-with-uncle-sam-taxes-fees-and-your-boat/. [Accessed: 14-Nov-2022].

[113] “Title 46 Chapter 1 Subchapter 1 Part 91 - Inspection and Certification,” *Code of Federal Regulations*, 01-Oct-2012. [Online]. Available: https://www.ecfr.gov/current/title-46/chapter-I/subchapter-I/part-91. [Accessed: 14-Nov-2022].

[114] “470 Class Rules 2022,” *World Sailing Class Association*, 01-Feb-2022. [Online]. Available: https://d7qh6ksdplczd.cloudfront.net/sailing/wp-content/uploads/2022/03/19014213/470_CR_20220201.pdf. [Accessed: 14-Nov-2022].

[115] R. García-Mayoral and J. Jiménez, “Drag reduction by Riblets,” *Philosophical Transactions of the Royal Society A: Mathematical, Physical and Engineering Sciences*, vol. 369, no. 1940, pp. 1412–1427, Apr. 2011.

[116] “Rules for Offshore Racing 2020 V1.0,” *American Power Boat Association*, 26-Jun-2020. [Online]. Available: https://www.apba.org/documents/1305915403-06262020-2020%20APBA%20Offshore%20Rules%20amended%2006.26.2020pdf.pdf. [Accessed: 14-Nov-2022].

[117] J. Baenen, “3M Hopes Stars & Stripes’ Success Will Boost Plastic Product With AM-America’s Cup-Sponsors,” *AP NEWS*, 05-Feb-1987. [Online]. Available: https://apnews.com/article/7593cedd8df4e6d218f3aae9bfdacb14. [Accessed: 14-Nov-2022].

[118] B. Evans and C. Thompson, “3M reveals successful collaboration with BMW Oracle Racing for 33rd America's Cup Match,” *3M News Center*, 04-Feb-2010. [Online]. Available: https://news.3m.com/2010-02-24-3M-Reveals-Successful-Collaboration-with-BMW-ORACLE-Racing-for-33rd-Americas-Cup-Match. [Accessed: 14-Nov-2022].

[119] J. Harvey, “How Much Does a Cigarette Boat Cost: Latest Prices in 2022,” *Boating Basics Online*, 02-Oct-2022. [Online]. Available: https://www.boatingbasicsonline.com/how-much-does-a-cigarette-boat-cost/. [Accessed: 14-Nov-2022].

[120] “Cigarette boats for sale,” *Yacht World*. [Online]. Available: https://www.yachtworld.com/boats-for-sale/make-cigarette/. [Accessed: 14-Nov-2022].

[121] “Cigarette powerboats for sale by owner,” *Powerboatlistings.com*. [Online]. Available: https://www.powerboatlistings.com/cigarette/. [Accessed: 14-Nov-2022].

[122] “42' X,” *Cigarette Racing*. [Online]. Available: https://www.cigaretteracing.com/boats/42-x. [Accessed: 14-Nov-2022].

[123] “Dockage Rates at Liberty Harbor Marina,” *Liberty Harbor Marina*, 05-May-2022. [Online]. Available: https://www.libertyharbormarina.com/dockage-rates/. [Accessed: 14-Nov-2022].

[124] “About Finsulate Antifouling,” *Finsulate*, 19-Jul-2021. [Online]. Available: https://www.finsulate.com/en/about-finsulate/. [Accessed: 14-Nov-2022].

[125] D. J. Kim, S. Y. Kim, Y. J. You, K. P. Rhee, S. H. Kim, and Y. G. Kim, "Design of high-speed planing hulls for the improvement of resistance and seakeeping performance," *International Journal of Naval Architecture and Ocean Engineering*, vol. 5, no. 1, pp. 161–177, 2013.

[126] A. Reza Kohansal and H. Ghassemi, "A numerical modeling of hydrodynamic characteristics of various planing hull forms," *Ocean Engineering*, vol. 37, no. 5-6, pp. 498–510, Apr. 2010.

[127] "New hull coatings for Navy ships cut fuel use, protect environment," *EurekAlert!*, 04-Jun-2009. [Online]. Available: https://www.eurekalert.org/news-releases/527620. [Accessed: 14-Nov-2022].

[128] "Antifouling Paints in Washington State Report and Recommendations," *Washington State Department of Ecology*, Sep-2019. [Online]. Available: https://apps.ecology.wa.gov/publications/documents/1904020.pdf. [Accessed: 14-Nov-2022].

[129] "Which Bottom Paint Should I Use?," *TotalBoat*, 19-May-2022. [Online]. Available: https://www.totalboat.com/2021/03/23/which-bottom-paint-should-i-use/. [Accessed: 14-Nov-2022].

[130] "Project, NP00946501-4: Safer Alternatives to Copper Antifouling Paints for Marine Vessels," *U.S. Environmental Protection Agency*, Jan-2011. [Online]. Available: https://pantheonstorage.blob.core.windows.net/environment/EPA-Funded-Alternatives-to-Copper-Based-Paint-Final-Report.pdf. [Accessed: 14-Nov-2022].

[131] A. O. Valkirs, P. F. Seligman, E. Haslbeck, and J. S. Caso, "Measurement of copper release rates from antifouling paint under laboratory and in situ conditions: Implications

for loading estimation to Marine Water Bodies," *Marine Pollution Bulletin*, vol. 46, no. 6, pp. 763–779, Mar. 2003.

[132] S. Pradhan, S. Kumar, S. Mohanty, and S. K. Nayak, "Environmentally benign fouling-resistant marine coatings: A Review," *Polymer-Plastics Technology and Materials*, vol. 58, no. 5, pp. 498–518, May 2018.

[133] M. S. Selim, M. A. Shenashen, S. A. El-Safty, S. A. Higazy, M. M. Selim, H. Isago, and A. Elmarakbi, "Recent progress in marine foul-release polymeric nanocomposite coatings," *Progress in Materials Science*, vol. 87, pp. 1–32, Feb. 2017.

[134] D. Akuzov, L. Franca, I. Grunwald, and T. Vladkova, "Sharply reduced biofilm formation from Cobetia Marina and in Black Sea water on modified siloxane coatings," *Coatings*, vol. 8, no. 4, p. 136, Apr. 2018.

[135] A. G. Nurioglu, A. C. Esteves, and G. de With, "Non-toxic, non-biocide-release antifouling coatings based on molecular structure design for Marine Applications," *Journal of Materials Chemistry B*, vol. 3, no. 32, pp. 6547–6570, Jun. 2015.

[136] E. R. Silva, O. Ferreira, P. A. Ramalho, N. F. Azevedo, R. Bayón, A. Igartua, J. C. Bordado, and M. J. Calhorda, "Eco-friendly non-biocide-release coatings for marine biofouling prevention," *Science of The Total Environment*, vol. 650, pp. 2499–2511, Feb. 2019.

[137] "Intersleek®," *international-marine.com*. [Online]. Available: https://www.international-marine.com/in-focus/intersleek. [Accessed: 06-Dec-2022].

[138] M. Lagerström, A.-L. Wrange, D. R. Oliveira, L. Granhag, A. I. Larsson, and E. Ytreberg, "Are silicone foul-release coatings a viable and environmentally sustainable alternative to

biocidal antifouling coatings in the Baltic Sea Region?," *Marine Pollution Bulletin*, vol. 184, p. 114102, Nov. 2022.

[139] "What is Sea Speed?," *sea-speed.com*. [Online]. Available: https://sea-speed.com/. [Accessed: 06-Dec-2022].

[140] "Sea-Speed," *https://www.seacoat.com/*. [Online]. Available: https://www.seacoat.com/product-2/. [Accessed: 06-Dec-2022].

[141] "Antifouling For Clean and Healthy Waterways," *Finsulate*, 24-Jan-2022. [Online]. Available: https://www.finsulate.com/en/. [Accessed: 14-Nov-2022].

[142] H. Breur, "EP1996453 (B1) - Antifouling Fibre Coating for Marine Constructions," *European Patent Office*, 10-Nov-2010. [Online]. Available: https://worldwide.espacenet.com/publicationDetails/biblio?CC=EP&NR=1996453B1&KC=B1&FT=D&ND=4&date=20101110&DB=&locale=en_EP. [Accessed: 14-Nov-2022].

[143] "Marine antifouling specialist Rik Breur receives European Inventor Award 2019 in the 'SMEs' category," *European Patent Office*, 20-Jun-2019. [Online]. Available: https://www.epo.org/news-events/press/releases/archive/2019/20190620c.html. [Accessed: 14-Nov-2022].

[144] "Speedgrade," *Finsulate*, 2021. [Online]. Available: https://www.finsulate.com/en/antifouling-products/speedgrade/. [Accessed: 14-Nov-2022].

[145] "Manufacturing Pressure-Sensitive Adhesive Products: A Coating and Laminating Process," *Adhesives Mag*, 01-Apr-2005. [Online]. Available:

https://www.adhesivesmag.com/articles/86079-manufacturing-pressure-sensitive-adhesive-products-a-coating-and-laminating-process. [Accessed: 14-Nov-2022].

[146] "Electrostatic Flocking," *American Flock Association*. [Online]. Available: https://www.flocking.org/about/electrostatic-flocking/. [Accessed: 14-Nov-2022].

[147] H. Andreae "Finsulate: Could this prickly antifouling revolutionise boat maintenance?," *Motor Boat & Yachting*, 10-Oct-2019. [Online]. Available: https://www.mby.com/maintenance/finsulate-prickly-antifouling-boat-maintenance-107759. [Accessed: 14-Nov-2022].

[148] "Engineering Material Nylon 12 Powder," *Formlabs*, 19-Aug-2020. [Online]. Available: https://formlabs-media.formlabs.com/datasheets/2001447-TDS-ENUS-0.pdf. [Accessed: 14-Nov-2022].

[149] L. Traub, "Calculation of Constant Power Lithium Battery Discharge Curves," *Batteries*, vol. 2, no. 2, p. 17, Jun. 2016.

[150] X. He, J.-P. Montillet, R. Fernandes, M. Bos, K. Yu, X. Hua, and W. Jiang, "Review of current GPS methodologies for producing accurate time series and their error sources," *Journal of Geodynamics*, vol. 106, pp. 12–29, Jan. 2017.

[151] "Knowing your boat means knowing its wake - department of primary ...," *Tasmanian Department of Natural Resources and Environment*, Oct-2015. [Online]. Available: https://nre.tas.gov.au/Documents/know-boat=know-wake-151014.pdf. [Accessed: 14-Nov-2022].

[152] "Principles of Ship Performance, Chapter 7," *United States Naval Academy*. [Online]. Available:

https://www.usna.edu/NAOE/_files/documents/Courses/EN400/02.07%20Chapter%207.pdf. [Accessed: 14-Nov-2022].

[153] K. Yousefi and A. Razeghi, “Determination of the critical Reynolds number for flow over symmetric NACA airfoils,” *2018 AIAA Aerospace Sciences Meeting*, pp. 1–11, Jan. 2018.

[154] “Silicone Fluid 350 TG,” *ChemDirect*. [Online]. Available: https://www.chemdirect.com/p/ChemD-3022-AMSI-350TG-2204-1x2204.6-Pounds-63148-62-9/silicone-fluid-350-tg-434749. [Accessed: 14-Nov-2022].